



Local tilt angle measurement of two-dimensional materials using LEEM

THESIS

submitted in partial fulfillment of the
requirements for the degree of

BACHELOR OF SCIENCE

in

PHYSICS

Author : Dennis Uitenbroek
Student ID : s1697552
Supervisor : Prof. dr. ir. Sense Jan van der Molen
MSc. Vera Janssen
2nd corrector : Prof. dr. ir. Tjerk Oosterkamp

Leiden, The Netherlands, July 6, 2018

Local tilt angle measurement of two-dimensional materials using LEEM

Dennis Uitenbroek

Huygens-Kamerlingh Onnes Laboratory, Leiden University
P.O. Box 9500, 2300 RA Leiden, The Netherlands

July 6, 2018

Abstract

A method to measure local tilt angles of two-dimensional materials in LEEM is developed. To create these local tilt angles graphene is stamped on top of pillars which are 55 nm high and 1 μm in diameter. The measurement method uses an aperture to select a spot on the sample and moved the sample to measure all over the sample. These spots are measured in diffraction space. By analyzing all diffraction images, a magnitude and an orientation of local tilt angles are obtained. The spatial resolution of this method is bound by the size of the aperture. In this experiment a spatial resolution of 338 nm is achieved. The angular resolution depends on the locating method of the diffraction spot. In this experiment an angular resolution of one degree is achieved.

Contents

| | | |
|----------|--|-----------|
| 1 | Introduction | 1 |
| 1.1 | Van der Waals materials | 2 |
| 1.1.1 | Transition Metal Dichalcogenide monolayers | 2 |
| 1.2 | A metal and semi-conductor in a single material | 3 |
| 1.3 | Measurement method | 3 |
| 2 | Experimental approach | 5 |
| 2.1 | Low energy electron microscopy (LEEM) | 5 |
| 2.1.1 | Electron optics & electron beam | 5 |
| 2.1.2 | Real space & diffraction space imaging | 7 |
| 2.2 | Diffraction space analysis | 8 |
| 2.2.1 | Distance between zeroth and first order diffraction spot | 8 |
| 2.2.2 | Movement of the diffraction spot | 9 |
| 2.2.3 | Angle determination | 10 |
| 3 | Measuring the local angle | 13 |
| 3.1 | Silicon as a ruler | 13 |
| 3.1.1 | Diffraction pattern of silicon | 14 |
| 3.2 | Aperture placement | 15 |
| 3.2.1 | Diffraction pattern around the sample | 16 |
| 3.3 | Finding the diffraction spot | 16 |
| 3.3.1 | Brightest pixel | 16 |
| 3.3.2 | Ellipse fit method | 17 |
| 3.3.3 | Gaussian smoothening then brightest pixel | 19 |
| 3.4 | Plotting the data | 20 |
| 4 | Sample fabrication & characterization | 23 |
| 4.1 | Sample fabrication | 23 |
| 4.1.1 | Substrate | 23 |
| 4.1.2 | Electron beam lithography | 23 |
| 4.1.3 | Graphene stamping | 24 |

| | | |
|----------|---|-----------|
| 4.2 | Sample design | 25 |
| 4.3 | Sample characterization using AFM & SEM | 25 |
| 4.3.1 | Flat area | 28 |
| 4.3.2 | Pillar one | 29 |
| 4.3.3 | Pillar two | 31 |
| 4.3.4 | Pillar three | 33 |
| 4.4 | Expected angle | 34 |
| 5 | Results | 37 |
| 5.1 | LEEM results | 37 |
| 5.1.1 | Flat area | 38 |
| 5.1.2 | Pillar one | 38 |
| 5.1.3 | Pillar two | 38 |
| 5.1.4 | Pillar three | 43 |
| 6 | Discussion | 47 |
| 6.1 | Flat area | 47 |
| 6.2 | Pillar one | 48 |
| 6.3 | Pillar two | 48 |
| 6.4 | Pillar three | 48 |
| 7 | Conclusion & outlook | 51 |

Chapter 1

Introduction

There is currently a huge interest in semiconductors. Semiconductors are at the basis of diodes, transistors and all modern electronics. Semiconductors have a lot of useful applications. They are used to be able to pass current in one direction more easily than the other direction, have variable resistance and be sensitive to light or heat. These properties are used for switching, amplification, energy conversion and making transistors.

To use semiconducting materials, they need to be attached to a metal. This metal ensures the supply or drain of current. Therefore there will always be a transition between a metal and a semiconductor.

The electronic junction between a metal and a semiconductor is always paired with the Schottky barrier [1]. This barrier is a potential barrier between these two materials. It is caused by the difference in electronic structure of the two materials. The band structure and the Fermi level are shown in figure 1.1.

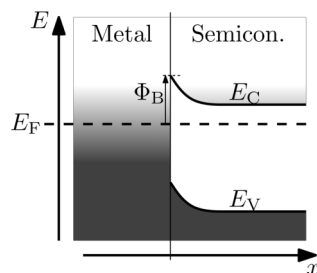


Figure 1.1: The Schottky barrier between a metal and a semiconductor is illustrated. The bandstructure of both materials are shown as well as the Fermi energy level.

This potential barrier causes unwanted heat, if a current flows through it, and therefore it is better to lower this barrier, also for device perfor-

mance. It has been shown that if both metal and semiconductor are made out of one material the Schottky barrier is lowered [2].

1.1 Van der Waals materials

To minimize electrical components two-dimensional materials, which are only one atomic layer thick, will be used to make a metal and a semiconductor out of one material. To understand this properly Van der Waals materials need to be understood first.

A Van der Waals heterostructure is a material which is composed of a stack of two-dimensional materials. These materials are always synthetically produced. The materials are bound by strong covalent bonds within each layer and a Van der Waals force between the layers. This results in a single material consisting out of multiple two-dimensional layers.

1.1.1 Transition Metal Dichalcogenide monolayers

Transition metal dichalcogenide monolayers (TMDs) are a specific type of Van der Waals materials. TMDs are two-dimensional materials which consist out of two different atoms. A transitional metal is sandwiched by chalcogen atoms, this forms a unit cell and this is expanded to create such a TMD monolayer. These materials can undergo a transition between two different structures of stacking. This stacking structure determines some electronic properties of the material. In the case of MoTe_2 , as in figure 1.2, the 2H phase is a semi-conducting state and the 1T' phase is a metallic state. The transition between the two structures is made by creating strain in the material [3] [4].

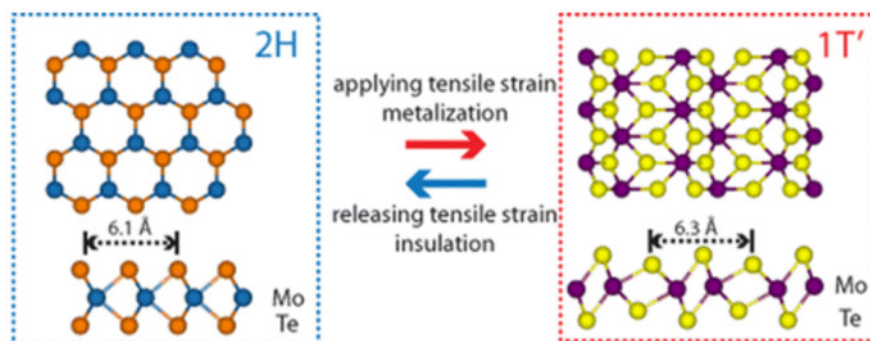


Figure 1.2: The two stacking phases of MoTe_2 . The 2H phase is a semi-conducting structure and the 1T' phase is a metallic structure. The transition between the two structures is made by creating strain in the material.[3]

1.2 A metal and semi-conductor in a single material

As described, MoTe₂ has both a metallic structure and a semi-conducting structure. In the future this will be used to create a single material which has both a metallic part and a semi-conducting part to lower the Schottky barrier between these two parts. To be able to do this first some fundamental properties need to be known about this material. To study the phase transition between the two structures a measurement setup is developed, shown in figure 1.3. This setup uses a drum of MoTe₂ and applies a voltage over the upper and lower part as in figure 1.3. This creates an attractive or repulsive force between the substrate and the drum, depending on the sign of the voltage. This force then creates strain in the drum and if this strain is large enough the drum transits to the 2H phase. So then there will be a metal-semi-conductor-metal system from the left to the right in the red two-dimensional material as in this figure.

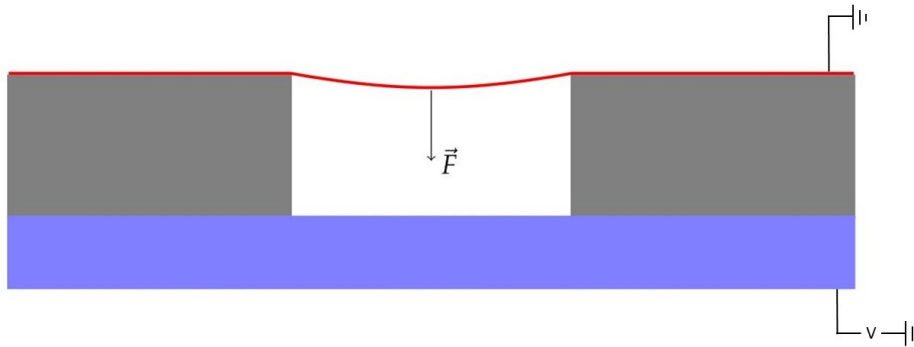


Figure 1.3: A cut of a drum to create strain in a monolayer. In red the monolayer, on top of the gray supporting material placed on a substrate (blue). Adapted from [5]

1.3 Measurement method

This strain is hard to measure since it is so small. The strain can also be measured via the curvature of the surface of the drum [6]. So to be able to determine the phase of MoTe₂ the curvature of the overhanging part needs to be known. To measure this curvature a local tilt angle measurement is developed in this thesis.

A low energy electron microscope is used, this microscope uses electrons which hit the surface. In this thesis a new measurement method for this angle measurement is developed. This technique is based on the work of Andringa [5] and uses his concepts to further develop the measurement.

This technique is developed using a flake of curved graphene in stead of a TMD drum. A TMD drum is harder to examine because the applied force creates an extra complexity factor. In further research TMDs will be re-searched using the developed technique.

Experimental approach

A method to measure the curvature of the surface is developed with curved multi-layer graphene using a low energy electron microscope. The principles of the microscope and what real space and diffraction space are are explained in this chapter. This results in the ability to measure tilt angles at the surface of the sample.

2.1 Low energy electron microscopy (LEEM)

To study two dimensional materials a low energy electron microscope (LEEM) is used. This microscope shoots electrons at a sample and measures the reflected electrons. The reflected electrons form an image and a diffraction pattern. The detector detects the reflected electrons. The switch between the image and the diffraction pattern is made by turning on/off a lens in the imaging column. The diffraction pattern changes when the atomic lattice changes. When the relative angle between the electrons and the surface changes, the diffraction pattern shifts. In the diffraction pattern every angle has its own position in the plane.

2.1.1 Electron optics & electron beam

A microscope is always diffraction limited, so when looking at small details a small wavelength is necessary. The wavelength of particles is given by the De Broglie wavelength and therefore electrons, with a thousand times smaller wavelength than visible light, are used in stead of visible light photons.

The necessary electrons are emitted by an electron gun with an energy of 15 keV. This is depicted in figure 2.1. The electrons then come across several electrostatic lenses and are bended by the magnetic prism array (MPA). The

first prism bends the electrons from the vertical column towards the sample. This is caused by a Lorentz force due to the magnetic field in the prism. Also between the prism and the sample there are again several lenses. Then right before the electrons interact with the sample they get slowed down. There is an adjustable potential difference between the final lens (the objective lens) and the sample, this is set on the sample. This difference can be adjusted up to $15 \text{ keV} \pm E_0$, where E_0 is 0-100 eV. So by changing this potential difference the landing energy of the electrons is changed.

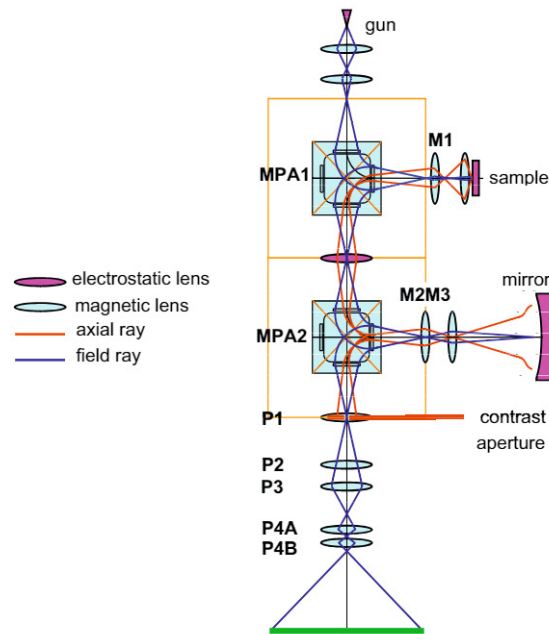


Figure 2.1: A simplified LEEM, with aberration corrections due to the second horizontal arm. [7] [8]

After interacting with the sample the electrons get accelerated again by the same potential difference between the last lens and the sample up to roughly 15 keV. The electrons go through the same lenses and again come across the prism, and bend downwards as seen in figure 2.1. They bend downwards due to the Lorentz force of the magnetic field in the prism. The electrons continue in the vertical direction, come across an electrostatic lens and enter the second prism.

The purpose of the second horizontal arm, as in figure 2.1, is to correct for spherical and chromatic aberrations. Spherical aberrations occur in each lens and are just a property of each lens. Chromatic aberrations occur because there is a little spread in kinetic energy of the electrons. The second horizontal arm gets rid of this by a symmetry argument. There are again

two magnetic lenses (M2 and M3) to be able to change the focus of the beam. The electrons reflect at the mirror which cancels out the lowest order aberrations.

After interaction with the sample and the aberration correction the only thing left is to create an image. The vertical part after the second prism is called the imaging column. It consists out of several lenses to focus the beam onto the detector plate (green plane in figure 2.1). By changing these lenses the focus can either be on the real space plane or be on the diffraction space plane. [7] [8]

2.1.2 Real space & diffraction space imaging

The objective lens in the LEEM focuses electrons. The path of the reflected electrons is schematically shown in figure 2.2. After the lens there exist a diffraction plane and a real space plane. The real space plane is the plane in which the electrons coming from one location at the sample focus. The diffraction plane is the plane in which the electrons leaving the sample with a certain angle focus together.

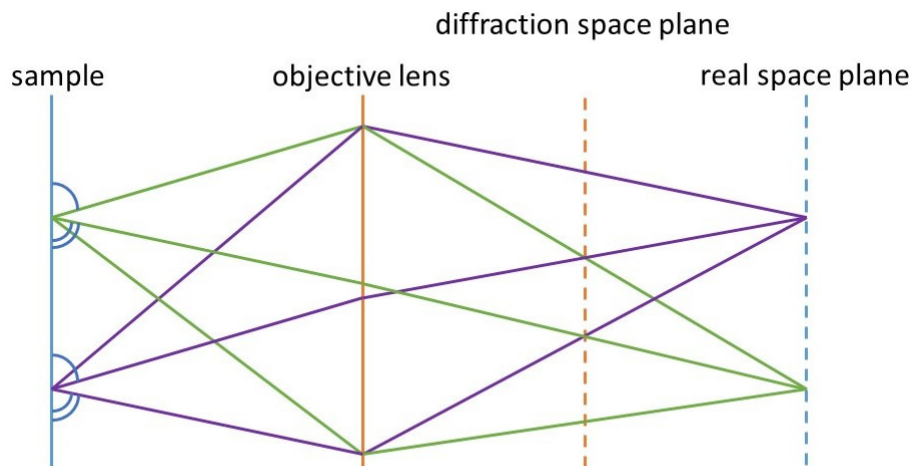


Figure 2.2: The objective lens in the LEEM creates a diffraction plane and a real space plane. The diffraction plane has electrons leaving the sample with the same angle at a certain spot. The real space plane focusses electrons leaving the sample from the same position.

The focus of the imaging column can either be on the diffraction plane or on the real space plane. The real space focus gives an enlarged view of

the sample. The diffraction space focus shows the diffraction pattern of the reflected electrons.

2.2 Diffraction space analysis

The diffraction space image made in LEEM contains two parts of information. The first part is the distance between the zeroth and the first order diffraction spot. The second part is the movement (location) of the diffraction pattern.

2.2.1 Distance between zeroth and first order diffraction spot

The distance between the zeroth and first order diffraction spot is a distance caused by Bragg's law. A hexagonal lattice is used and this gives rise to a correction factor.

Bragg's law

Electrons approach the surface of the flake. The electrons hit the atoms at the surface and get scattered in all directions. The scattered electrons will interfere with each other. The interference will alternate between constructive and destructive. In figure 2.3 the scattering under an angle θ is shown. In this figure d is the in-plane lattice constant.

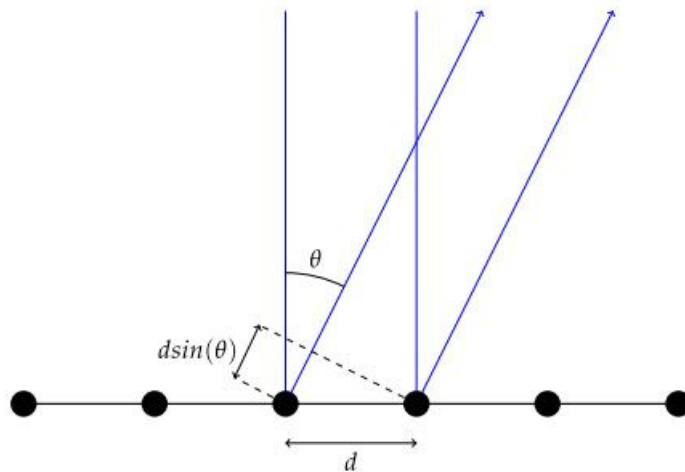


Figure 2.3: Electron waves are scattered by the atomic lattice, with lattice constant d . This happens under an angle θ . After scattering the electrons interfere with each other. [5]

Whether the interference of the electrons will be constructive or destructive depends on the $d \sin(\theta)$ term. This term determines the difference between the two paths. If this path difference is an integer times the wavelength the interference will be constructive. So to find the diffraction spots equation 2.1 needs to be satisfied.

$$d \sin(\theta) = n \lambda \quad (2.1)$$

In this equation is d the in-plane atomic lattice constant, θ is the direction in which the electrons are scattered, n is the n^{th} order diffraction spot and λ is the wavelength of, in this case, the electrons.

Hexagonal lattice

Since the surface of the material is studied by low energy electrons the lattice is characterized by two lattice vectors. These in-plane real space lattice vectors are called \mathbf{a} and \mathbf{b} in real space. Since the angle is calculated from diffraction space these vectors need to be converted into reciprocal lattice vectors. These reciprocal lattice vectors are: \mathbf{a}^* and \mathbf{b}^* . The relation between real space and reciprocal lattice vectors is [9]:

$$\mathbf{a}^* = \frac{2\pi \mathbf{b} \times \hat{\mathbf{n}}}{|\mathbf{a} \times \mathbf{b}|}, \quad \mathbf{b}^* = \frac{2\pi \mathbf{a} \times \hat{\mathbf{n}}}{|\mathbf{b} \times \mathbf{a}|} \quad (2.2)$$

Graphene has a hexagonal lattice and therefore both in-plane lattice constants are of equal size: $a = |\mathbf{a}| = |\mathbf{b}| = b$. These lattice constant make an angle of $\frac{\pi}{3}$ w.r.t. each other. This leads to the length in diffraction space of:

$$|\mathbf{a}^*| = |\mathbf{b}^*| = \frac{2\pi a}{a^2 \sin(\frac{\pi}{3})} = \frac{2\pi}{a \frac{1}{2}\sqrt{3}} \quad (2.3)$$

So there is an additional factor of $\frac{\sqrt{3}}{2}$ which needs to be taken into account.

2.2.2 Movement of the diffraction spot

The diffraction pattern contains information about the surface of the material. The location of the diffraction pattern determines the tilt angle of the sample. This movement is therefore used to reproduce the tilt angle of the sample.

Electron interaction with a tilted sample

As stated in subsection 2.1.1 the electrons interact with the sample in the first horizontal arm of the LEEM. The electrons are scattered after interaction with an atom. The scattered electrons will then interfere with each

other and create an interference pattern, as described in Bragg's law part (subsection 2.2.1). When the LEEM is focused on diffraction space this interference pattern becomes visible.

If the sample is tilted there is another effect on top of that, as illustrated in figure 2.4. The tilt causes a change in the direction of the reflected angles of 2α . So all diffraction spot angles are rotated over 2α . In diffraction space this means that all diffraction spots are shifted by the same distance. This shift in distance corresponds to an angular shift of 2α . Thus half this shifted distance corresponds to the tilt angle α .

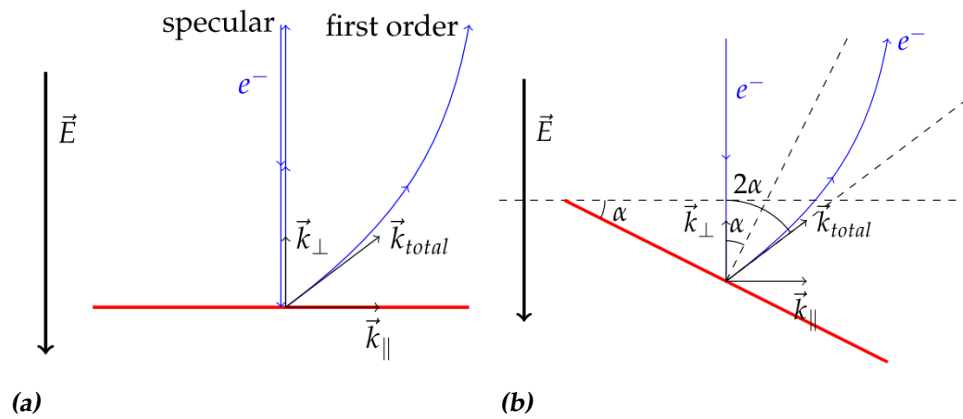


Figure 2.4: Two ways to reflect electrons, determined by the angle of incidence. (a) Electrons approaching the sample vertical ($\alpha = 0$) are reflected without changing the angle of the zeroth order diffraction spot. (b) Electrons approaching the sample at a certain angle ($\alpha \neq 0$) are reflected at twice this angle. [5]

The electrons coming from the sample are all exposed to the potential difference between the sample and the first lens. Therefore they follow a parabolic path after leaving the sample in the direction of the energy. The parabolic paths are visible both in figure 2.4a and in figure 2.4b.

2.2.3 Angle determination

The sample tilt needs to be expressed quantitatively. This is done by combining Bragg's law together with the electron interaction with a tilted sample.

In figure 2.4b the zeroth order diffraction spot is rotated with an angle of 2α . From this image equation 2.4 can be derived using trigonometry.

$$\sin(2\alpha) = \frac{k_{\parallel}}{k_{tot}} \quad (2.4)$$

In equation 2.4 is k_{tot} related to the landing energy of the electron. The dispersion relation can be determined using quantum mechanics and holds:

$$k_{tot} = \frac{\sqrt{2mE}}{\hbar} \quad (2.5)$$

Here is m the electron mass, E the landing energy of the electron and \hbar the reduced Planck constant. The dispersion relation can be combined with equation 2.1; Bragg's law. The wavelength and the total momentum are related to each other as: $k_{tot} = \frac{2\pi}{\lambda}$.

$$\frac{\sqrt{2mE}}{\hbar} = k_{tot} = \frac{2\pi}{\lambda} = \frac{d \sin(\theta)}{n 2\pi} \quad (2.6)$$

This can be rewritten as:

$$\theta = \arcsin\left(\frac{2\pi\hbar}{\sqrt{2mE}} \frac{n}{d}\right) \quad (2.7)$$

In this equation θ is the angle the electrons leave the sample when creating the n^{th} order diffraction spot. The incoming electrons have energy E and mass m . The material has in-plane lattice constant d .

Chapter 3

Measuring the local angle

The local measurement of angles in LEEM is explained in this chapter. First, another sample is needed to convert distances in diffraction space into a real space angle. Then, for the tilt measurements, an aperture is placed to select a spot on the curved graphene sample. Both diffraction and real space information is combined to obtain a local tilt angle measurement.

3.1 Silicon as a ruler

The used sample, multi-layered graphene, had its first order diffraction spots outside the field of view. Therefore another sample, with a larger unit cell, can be used as a ruler.

Different lattice constants have different angles with constructive interference, see equation 2.7. This results in different distances in diffraction space. This concept is used to determine the angles of the graphene flake. The specific angle of silicon needs to be translated to graphene. The ratio of the two distances in diffraction space is equal to the ratio of the two angles θ of the two different materials; as in equation 3.1.

$$\frac{\theta_{Gr}}{a_{Gr}} = \frac{\theta_{Si} / \sin(\frac{\pi}{3})}{s_{Si}} \quad (3.1)$$

With s_{Si} being the distance between the zeroth and first order diffraction spot of silicon. a_{Gr} is the movement of the zeroth order diffraction spot of graphene. The specific angle of silicon (θ_{Si}) can be calculated with equation 2.7, s_{Si} is constant and can be measured in a diffraction image of silicon. The only variable is: a_{Gr} ; this distance will vary all over the sample meaning that there is local tilt. Because silicon has a hexagonal lattice and the distance between the zeroth and first order diffraction spot is measured, this distance need to be corrected by a factor of $\sin(\frac{\pi}{3})$. For graphene only

the movement of the zeroth order diffraction spot is used, so there is no need for a correction factor there.

This together holds the equations below:

$$\theta_{Gr} = \frac{\theta_{Si} a_{Gr}}{\sin(\frac{\pi}{3}) s_{Si}} \quad (3.2)$$

$$= \arcsin\left(\frac{2\pi\hbar}{\sqrt{2mE_{Si}}} \frac{n_{Si}}{d_{Si}}\right) \frac{a_{Gr}}{\sin(\frac{\pi}{3}) s_{Si}} \quad (3.3)$$

$$\alpha_{Gr} = \frac{1}{2} \arcsin\left(\frac{2\pi\hbar}{\sqrt{2mE_{Si}}} \frac{n_{Si}}{d_{Si}}\right) \frac{2 a_{Gr}}{\sqrt{3} s_{Si}} \quad (3.4)$$

α_{Gr} is the angle the graphene makes w.r.t. flat. The last step from equation 3.3 to 3.4 is because the reflected angle is twice the angle of the graphene w.r.t. flat.

3.1.1 Diffraction pattern of silicon

Figure 3.1 shows the diffraction pattern of silicon(111) as measured in LEEM. This is used to determine the distance between the zeroth and first order diffraction spot. Arrows are drawn pointing at the visible first order spots. The average length of these lines is taken to be the distance s_{Si} .

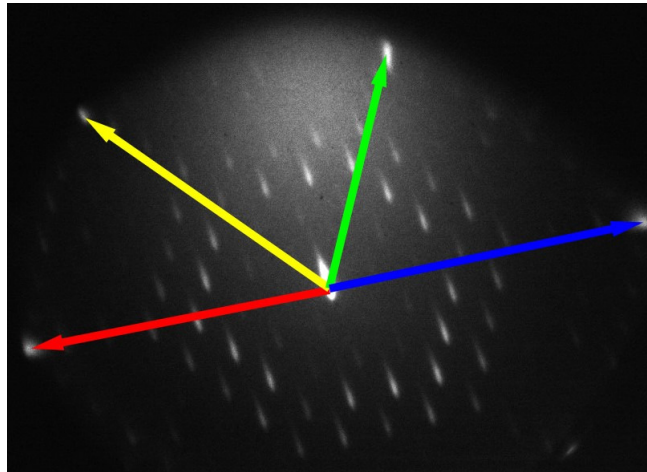


Figure 3.1: The diffraction pattern of silicon(111) as seen in LEEM in diffraction mode. Colored arrows are added pointing at each visible first order diffraction spot. In between the zeroth and first order diffraction spot six more spots are visible. These are caused by the 7×7 reconstruction of silicon(111)

In this figure not only the zeroth and first order spots are visible. In between are six less bright spots, not all of them are visible. These spots

are caused by the 7×7 reconstruction of silicon(111). This pattern was visible at a landing energy of 14.9 eV. The length of each arrow (in pixels) is displayed in table 3.1.

| Line | length (pixels) |
|---------|-----------------|
| Red | 390 |
| Yellow | 384 |
| Green | 308 |
| Blue | 410 |
| Average | 373 |

Table 3.1: Length of the arrows pointing from the zeroth to the first order diffraction spot. The average is calculate in order to be able to measure the tilt angles of graphene.

Now the conversion factor for angles of graphene is calculated. Silicon(111) has in-plane lattice constant: $d_{Si} = 5.407\text{\AA}$ [10]. This is done using equation 3.4.

$$\alpha_{Gr} = \frac{1}{2} \arcsin\left(\frac{2\pi\hbar}{\sqrt{2m} 14.9} \frac{1}{5.407}\right) \frac{2}{\sqrt{3} 373} a_{Gr} \quad (3.5)$$

$$= 0.0554 a_{Gr} \quad (3.6)$$

This allows us to calculate the tilt angle of graphene. If the distance the zeroth order spot moves (in pixels) is multiplied by 0.0554 the tilt angle is obtained in degrees.

3.2 Aperture placement

The diffraction pattern is always the diffraction pattern of the irradiated area on the sample. Therefore the spatial resolution of the angle measurement is more local when the irradiated area is smaller. Thus by decreasing the size of the irradiated area the angle can be measured of smaller areas. The decreasing of the irradiated area is done by placing an aperture in one of the real space planes in the incoming beam. This aperture selects a spot in real space and then the angle of this spot can be calculated as described in section 3.1.

3.2.1 Diffraction pattern around the sample

Since now only one spot is selected by the aperture, the aperture needs to move around the sample. The movement of the aperture has a major disadvantage. The aperture has micrometer screws driven by hand. This makes the movement very inaccurate. The aperture ensures also that the electrons at the irradiated part will always come in with the same angle. The only thing that matters is the relative motion between the aperture and the sample. To not suffer from this disadvantage the aperture is held at the same position and the sample is moved around. The sample holder is driven by piezoelectric motors. This makes the movement a lot more accurate and the result reproducible.

After the measurement the locations of where the aperture has been needs to be reconstructed. The motors step in a sequence which forms a square. This is recorded in real space. Next the aperture is placed in position and an image of the aperture is taken in real space. With this image the location of the aperture in each frame of the sequence is determined. The size of the aperture can be measured with this image too. After determining the location of the aperture the LEEM is switched to diffraction mode. Then the same square sequence is repeated. So this results in having a diffraction pattern at each spot where the aperture has been.

3.3 Finding the diffraction spot

The location of the diffraction spot is determined by a home build python program. This program has three different ways to determine the location of the spot. They all have their advantages and disadvantages.

3.3.1 Brightest pixel

The first method is the brightest pixel method. This method takes the brightest pixel of the image to be the central location of the diffraction spot. The zeroth order diffraction spot will contain the brightest pixel of the image. The advantage is that it is a relatively easy and fast way to detect the spot. The disadvantage is that if there is a dead pixel on the detector plate, this pixel will always be the brightest pixel. In this experiment however this is never the case. This method is also noise sensitive.

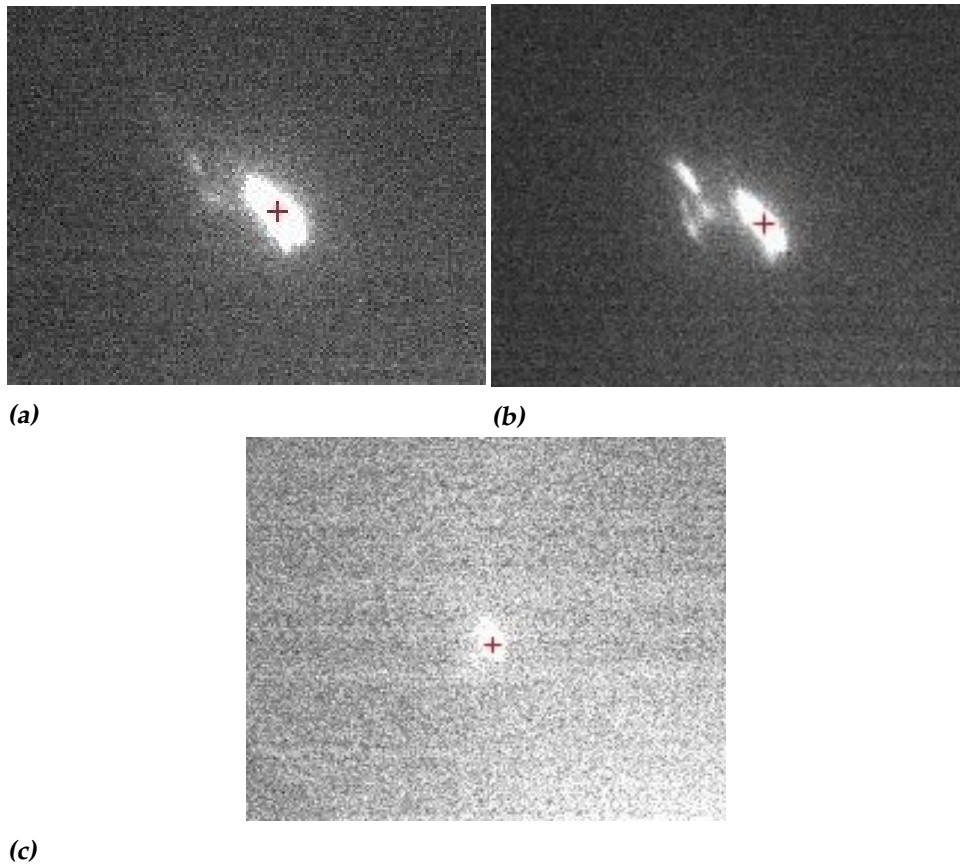


Figure 3.2: (a) A single spot detected by taking the brightest pixel. (b) Multiple spots, the brightest is detected. (c) A less intense single spot, still a pixel inside the spot is detected.

In figure 3.2 can be seen that this method always detects a pixel in the spot. This is not necessarily the center of the spot. The dead pixel problem is also still there, it just never happened taking the diffraction images.

3.3.2 Ellipse fit method

The second method is to fit an ellipse around the zeroth order diffraction spot. Then the center of the ellipse is chosen to be the center of the spot. This in theory sounds as a good way to characterize the diffraction spot. This method does use the information of the whole diffraction spot and therefore is more accurate in finding the center than only taking the brightest pixel. In practice this method detects a lot more spots than detected by eye. Sometimes also the true spot is not even detected.

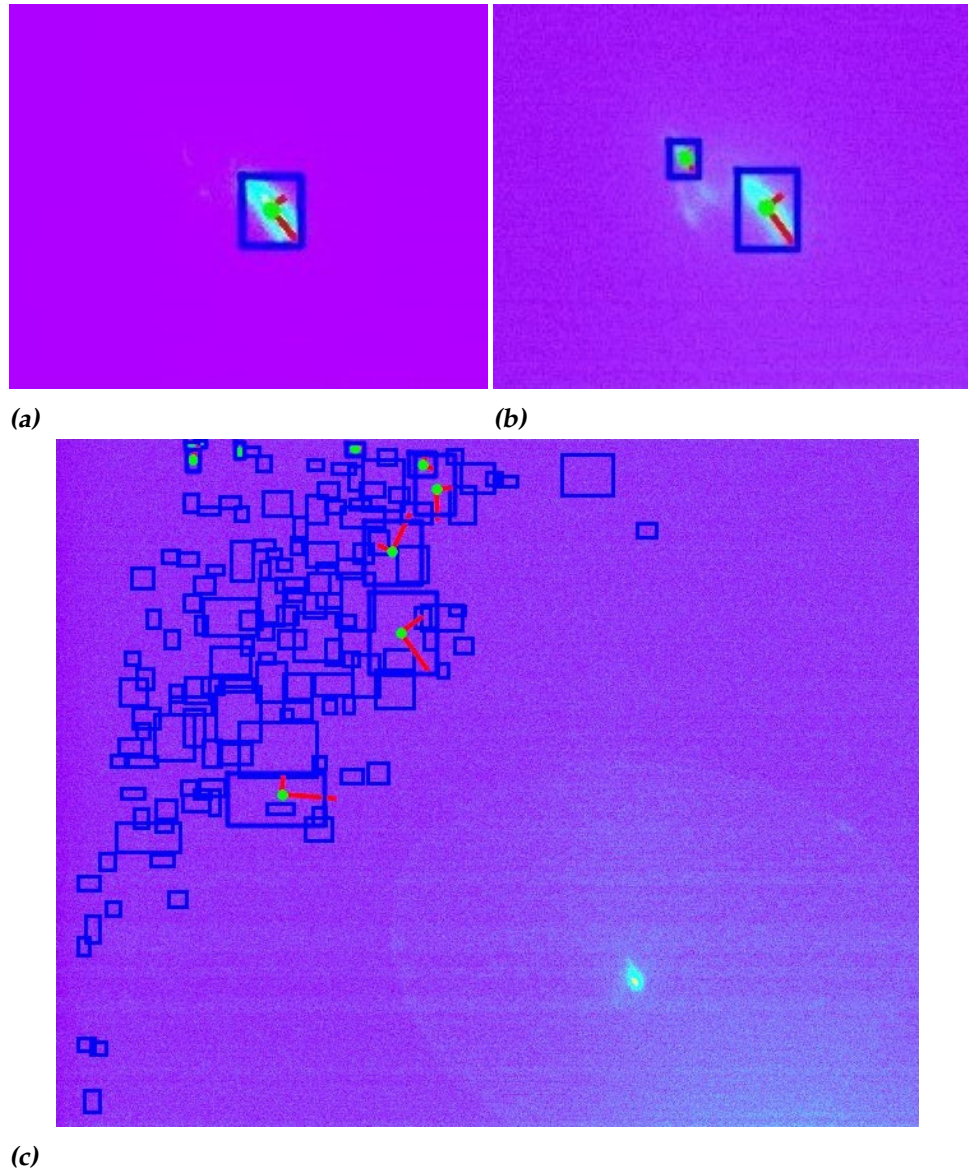


Figure 3.3: The ellipses fitted to some diffraction images. The blue rectangle is the found region of interest, the green dot is the center of the ellipse and the two red axis are the minor and mayor axis of the ellipse. (a) A single spot detected by taking the ellipse fit. (b) Multiple spots, detected by fitting ellipses. (c) A less intense single spot, detected wrong by the ellipse fit method.

In figure 3.3 are the diffraction spots detected by the ellipse fit method visible. The blue region is the region the algorithm searches for an ellipse. These regions are detected automatically. The green dot is the detected center of the ellipse and the red lines are the minor and mayor axis of the ellipse. Figure 3.3c shows a wrong detection of the diffraction spot. In this

case there is only one diffraction spot, which is clearly visible by eye. This detection of the wrong location also happens when there are multiple spots visible.

3.3.3 Gaussian smoothening then brightest pixel

The third method is to first gaussian smoothen the image and then take the brightest pixel. The gaussian smoothening algorithm looks at a pixel and compares it to its neighbors. Then the value of the pixel is adjusted to a gaussian fit of the pixel and its neighbors. The function used to do this is `GaussianBlur` from the `OpenCV2` package in python. The fit parameters of the gaussian can all be set in this function. The sigma of the fitting gaussian can be set. For this experiment an sigma of two was used in both X and Y direction. This value let enough details intact and smoothed enough as determined by eye.

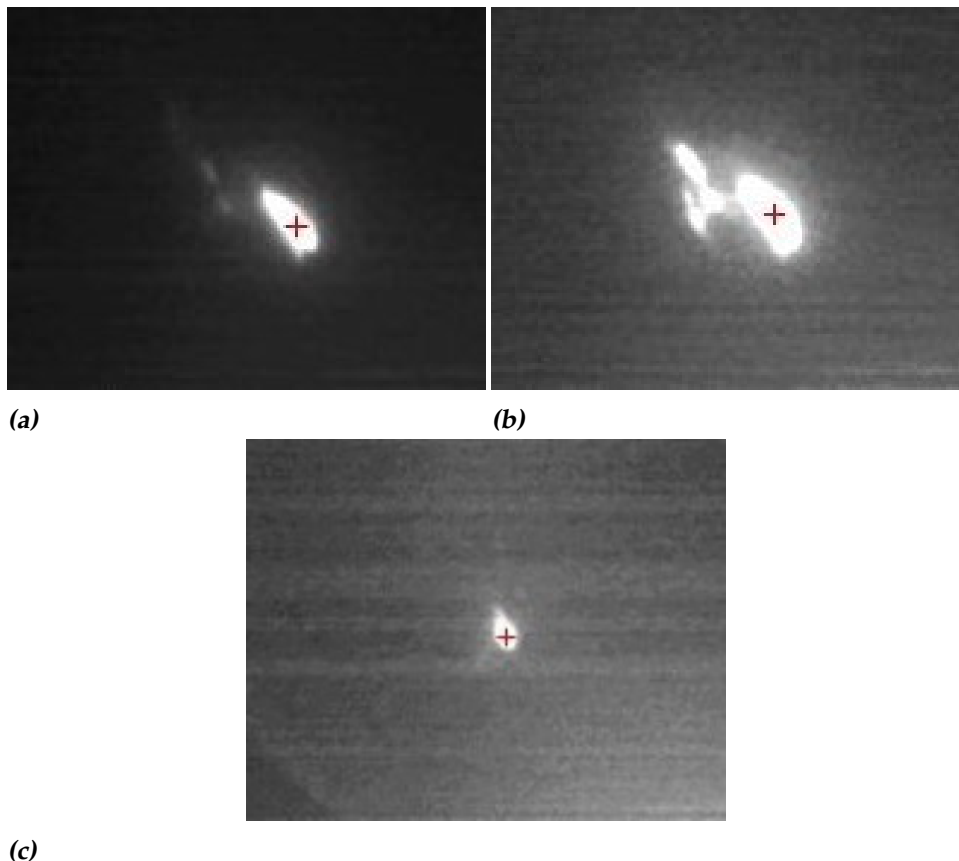


Figure 3.4: (a) A single spot gaussian smoothed and detected by taking the brightest pixel. (b) Multiple smoothened spots, the brightest is detected. (c) A less intense smoothened single spot, correctly detected.

Figure 3.4 shows the detection of the brightest pixel after gaussian smoothing the image. The detected location is always in the spot and is very often at the center of the spot as detected by eye. This makes the smoothing method the most reliable and therefore this one is used to analyze the LEEM data.

3.4 Plotting the data

In order to be able to plot an angle, flat needs to be defined. This is done by looking in the real space data and deciding which frame has the aperture at a location where the flake is flat. This is mostly the case if the aperture is far away from the pillar.

Then the location of the corresponding diffraction spot is set as flat. The next step is to look where all other spots are w.r.t. this location. These relative locations contain two types of information. The first is the distance between the two points and the second is the angle the two make w.r.t. each other. The spatial shift in diffraction space is caused by a tilt angle. The direction of the shift depends on the orientation of the tilt angle. The distance is converted to an angle using equation 3.6. This is the magnitude of the angle in real space. This is schematically illustrated in figure 3.5.

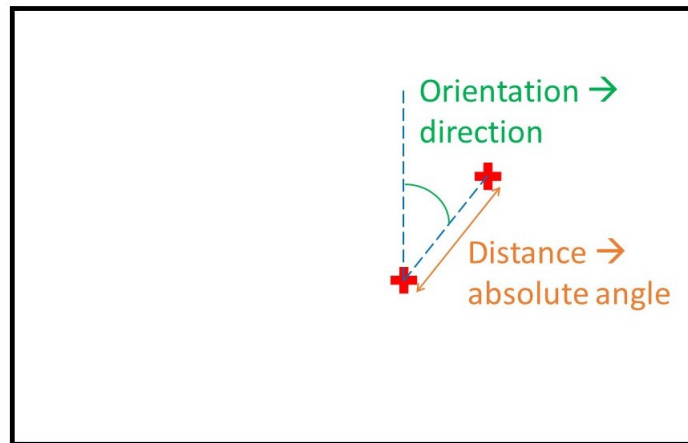


Figure 3.5: Two detected locations of the diffraction spot marked by red crosses. The distance between them is converted to an absolute angle (magnitude) using equation 3.6. The orientation they have w.r.t. each other is the direction of the angle.

The angle the two locations make w.r.t. each other is used to determine the direction of the angle. This is done by setting a vertical line in the

upward direction from the location of the flat spot. The direction is then determined by calculating the angle between this vertical and the found diffraction spot, as shown in figure 3.5. This direction runs from -180° to 180° . There is a choice in setting the zero degree direction and therefore an arbitrary rotation remains in the direction plot. Both magnitude and direction are plotted separately and together as vectors for each plot.

The measuring process used an algorithm to take images in a square lattice. This was done by setting the piezoelectric motors each time w.r.t. their current position. This resulted in one tilted axis and thus the square became a rhombus. This was noted after the measurement of pillar two and the code was improved to correct for this. The improvement was based on setting the start value of the slow axis after each fast row. This resulted in a nearly square lattice as can be adapted from figure 5.4.

Sample fabrication & characterization

In order to measure tilt angles in LEEM, tilted areas on a sample are necessary. The samples fabricated consist of an array of pillars on top of a substrate. This is done by electron beam lithography. On top of these pillars flakes of multi-layer graphene were stamped. The resulting samples are characterized using AFM and SEM.

4.1 Sample fabrication

4.1.1 Substrate

The substrate used is a silicon(100) wafer with native oxide on top. This wafer is diced in order to be able to fit it in the sample cap holders. The diced pieces were $6\text{ mm} \times 6\text{ mm}$.

4.1.2 Electron beam lithography

On top of the diced substrate the pillars were fabricated. The fabrication uses a process called electron beam lithography. This process is explained step by step in this paragraph.

On top of the diced substrate the resist ARP6200 is applied. This resist is applied by spin coating, the result is depicted in step 2 of figure 4.1.

The next step is to expose this substrate-resist combination to an electron beam. This electron beam is exposed on specific places. The beam changes the polymer on these places. The exposed resist is then placed in a development liquid (pentyl acetate, for 90 seconds). In development the exposed parts of the resist are dissolved. This is shown in step 3 of figure 4.1.

Next is the evaporation of two metals. First 5 nm of titanium is evaporated

to attach a sticking layer to the siliconoxide. Next 50 nm of gold is added on top. The titanium is in a crucible and is been irradiated with an electron beam. This electron beam heats up the titanium and the titanium evaporates. The titanium lands on the substrate and the resist, as shown in step 4. After the titanium the gold is evaporated in the same way. The gold is in a crucible and is irradiated at with an electron beam. The gold lands on top of the titanium as in step 5. The settings on the evaporation machine were 5 nm of titanium and 50 nm of gold. The last step is to lift off the resist. This is done by placing the substrate now in dimethyl fomamide. This process is done at 80 °C and takes one hour.

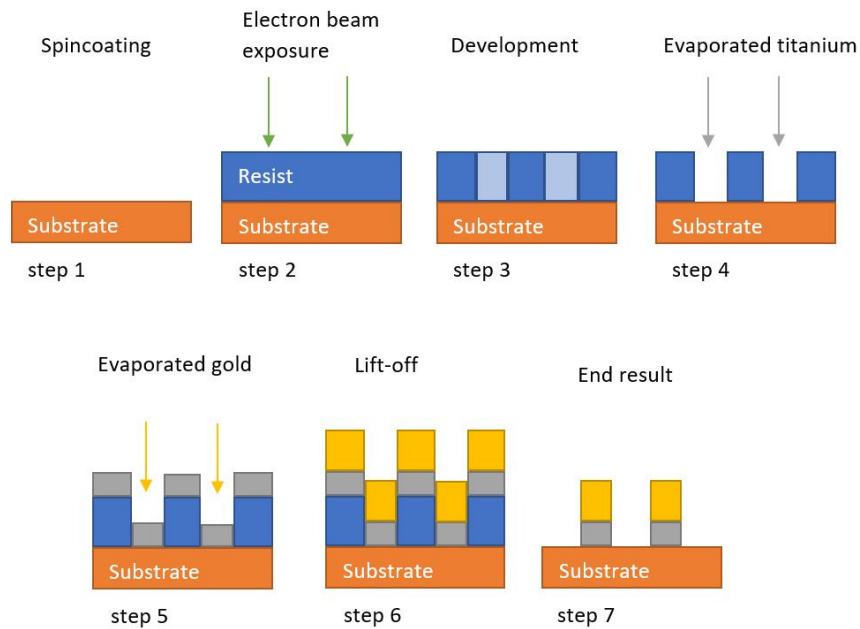


Figure 4.1: The electron-beam lithography process displayed in seven steps, used to create the desired pattern on the silicon.

4.1.3 Graphene stamping

After creating the desired pattern the graphene needs to be stamped. The graphene is separated from a bulk of graphite using the exfoliation technique. Exfoliation is done by taking a piece of tape and placing it on a bulk of graphite, then by pulling it off the graphite it will take some flakes of graphite off. Repeating this process several times ensures that the graphite will get thinner. After about five times there will be some flakes of multi-layer graphene on the tape.

The tape with flakes is placed on a piece of polydimethylsiloxane (PDMS). PDMS is transparent. The PDMS is placed on a glass plate in an optical microscope. With the optical microscope the flakes of graphene can be identified. A region with the desired flakes is searched. This region is then aimed at the pillars. This aiming is done with a micrometer screw controlled stage. When the flakes and the pillars are aligned the flakes are lowered on top of the pillars.

4.2 Sample design

The flake in this experiment needs to have a curved surface. In order to improve the chance of successfully making a sample not just one, but multiple pillars were made by lithography. In this experiment an array of ten by nine pillars is used. These pillars were one micrometer in diameter. The schematic view of the flakes on top of the pillars is shown in figure 4.2.

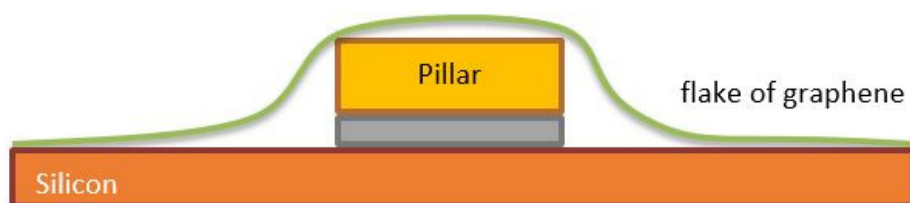


Figure 4.2: Schematic side view of a pillar with a flake on top of it (not to scale). The sizes are the sizes like in the electron beam design and the height is a setting of the evaporator.

The result of the fabrication is shown in figure 4.3. This image is taken with an optical microscope. The contrast in the picture is not the original contrast, the contrast is enhanced to be able to see the flakes clearly. The three flakes of graphene are visible as well as the array of pillars. The gold triangles in the corners are part of the markers. These markers were also made by lithography in order to ease the searching process in the microscopes.

4.3 Sample characterization using AFM & SEM

The created sample is characterized using atomic force microscopy (AFM) and scanning electron microscopy (SEM). One flat area and three pillars are chosen to apply the new angle measurement method to. For each pillar a height plot is made. With these height plots an average angle is calculated. An overview of two of the flakes of graphene is showed in figure 4.4.

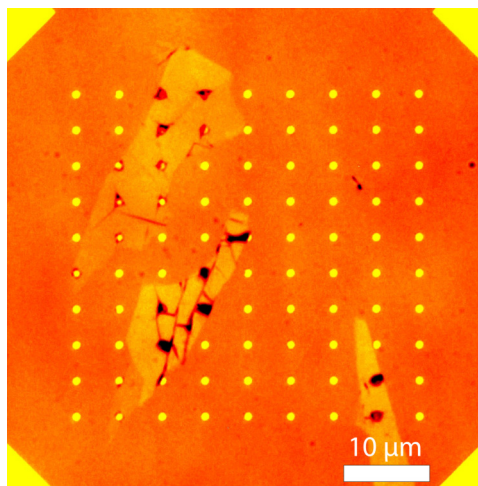


Figure 4.3: The result of the electron-beam lithography combined with stamping of graphene. This image is taken with an optical microscope, the contrast is enhanced to be able to see the flakes clearly. Three flakes of graphene are visible in the region with the array of pillars.

Figure 4.4 is made with SEM, the contrast is enhanced to see the flakes of graphene clearly.

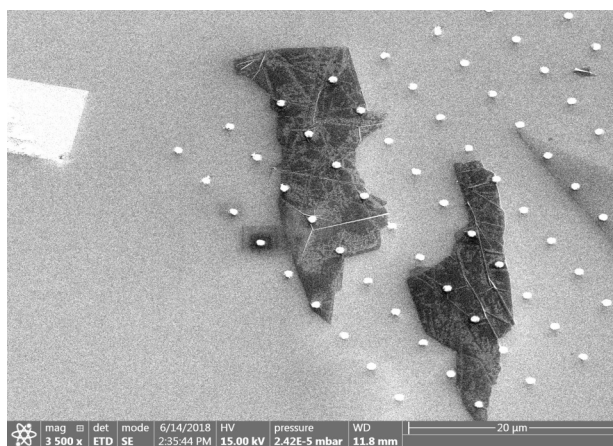


Figure 4.4: Overview of the two flakes of graphene on top of the pillars. This image is taken under 45° using SEM. The contrast in the image is enhanced to be able to see the flakes of graphene clearly.

The left flake in figure 4.4 is chosen for further investigation because more pillars are present underneath the left flake. An image of the error signal of the AFM measurement is depicted in figure 4.5. The error signal

is displayed, because this gives an enlarged view of reality. This image is rotated 90° w.r.t. figure 4.4.

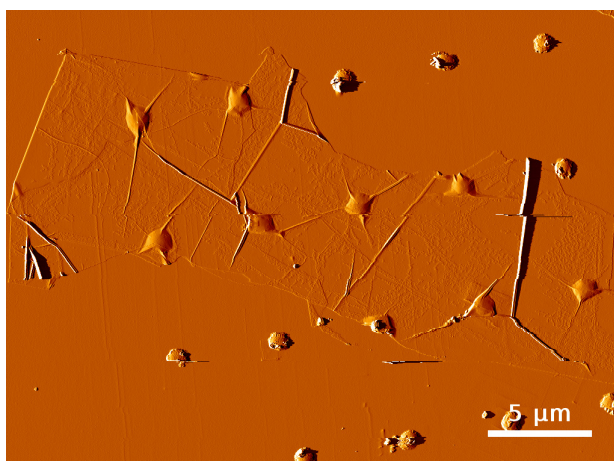


Figure 4.5: The AFM error signal provides an overview of the upper part of the left flake of figure 4.4. Measurement artifacts are visible as irregular horizontal lines. The scanning direction of the AFM was also horizontal in the image.

This AFM overview shows some straight horizontal lines. These are artifacts of the measurement. Also some lines are visible in a non-horizontal direction. These are interpreted as folding lines of the graphene flake. This is concluded because these lines are clearly higher than the rest of the flake, according to the AFM measurement. Another argument is both AFM and SEM measurements show these lines and therefore they are not an artifact of one of the two measurements.

Three pillars and a flat part, for a control measurement, were selected for the new measurement method. The chosen ones are illustrated in figure 4.6.

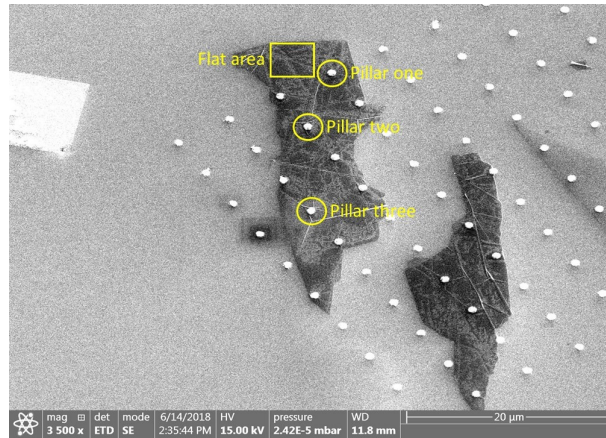


Figure 4.6: Overview made in SEM of the two flakes of graphene with the selected pillars and corresponding numbering. This image is taken under 45° in SEM, the contrast is enhanced to be able to see the flakes clearly.

For clarity the three pillars and the flat part markings are also added to the AFM image (figure 4.7).

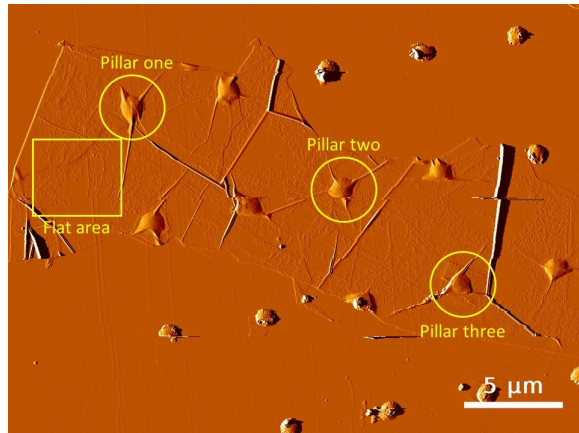


Figure 4.7: AFM overview of the left flake as in figure 4.6. The chosen pillars and flat area are displayed in the image. Measurement artifacts are visible as horizontal lines in the image.

Now each selected area will be investigated one-by-one. Eventually a height plot of each pillar is made. This is used to calculate an average angle.

4.3.1 Flat area

The flat area as pointed in figure 4.7 is characterized using AFM. This is shown in figure 4.8. This image has the same orientation as in figure 4.7.

Pillar one is half visible in the upper right corner of the AFM image of the flat area. The image shows a part of the substrate too. The flake shows irregularities all over. These are interpreted as carbon features as a residue of the graphene stamping.

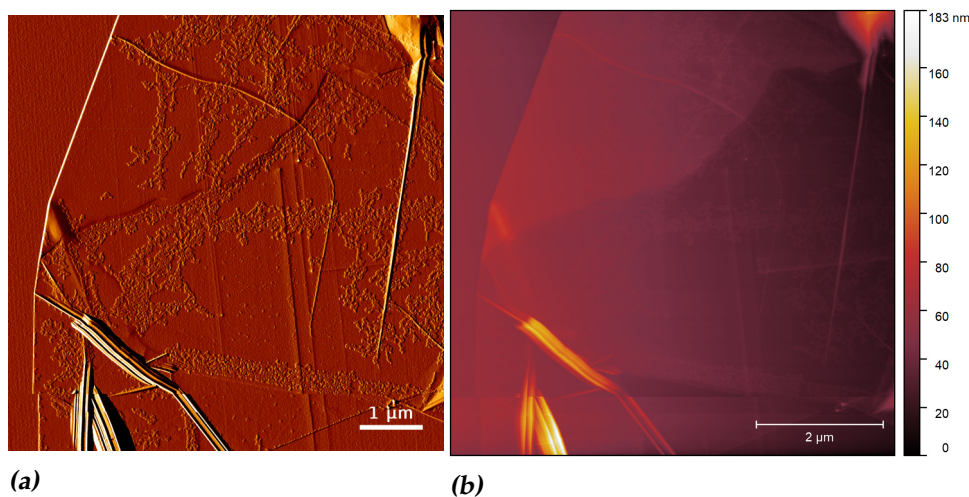


Figure 4.8: AFM images of the flat area. (a) The error signal of the measurement. (b) The height measurement of the flat area.

4.3.2 Pillar one

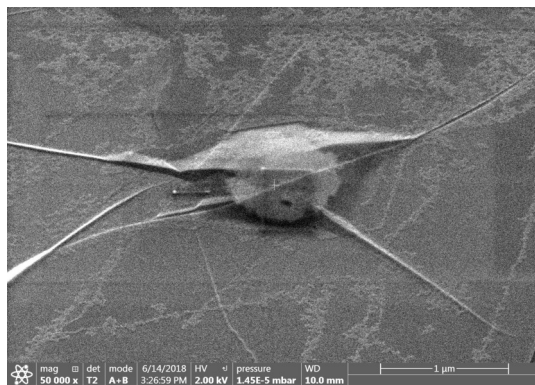
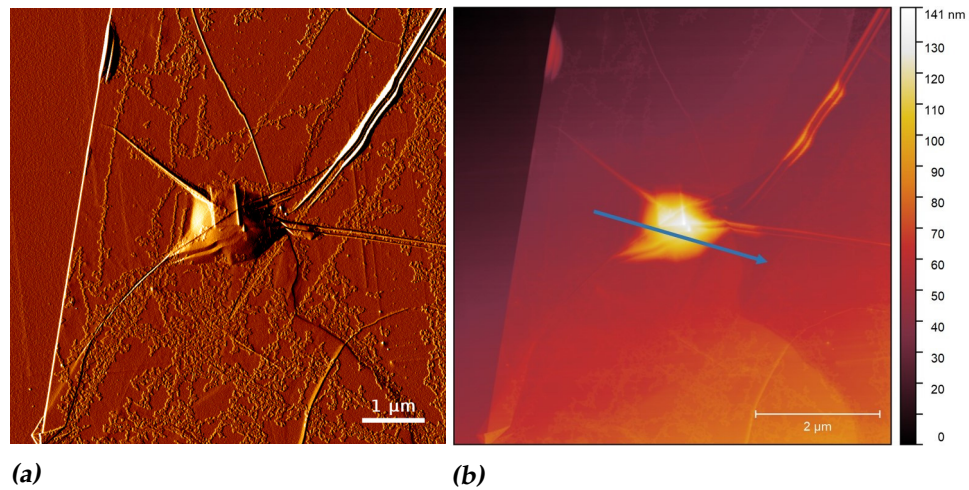


Figure 4.9: Pillar one with multi-layer graphene on top as seen in SEM, image taken under 45°. The contrast of the SEM image is enhanced to be able to see the details, such as the pillar, clearly.

Pillar one seen in SEM is shown in figure 4.9. In this image the pillar is visible as well as the graphene flake folding over it. It is visible that the graphene not always touches the pillar or substrate. The flake shows

irregularities, these are interpreted as carbon features as a residue of the graphene stamping. Also sharp straight lines are visible, these are interpreted as folding lines of graphene. The contrast in this image is enhanced to see the pillar, carbon features and folding lines clearly.

The same area is also characterized by AFM, see figure 4.10. The AFM image is 180° rotated w.r.t. figure 4.9. The carbon features are visible as well as the folding of the graphene. Some of the sharp lines appear double in the images. This is due to a measurement artifact, it appears when the surface is sharper than the AFM measurement tip. The blue arrow depicts the position and direction of the height plot across the pillar. The corresponding height plot is visible in figure 4.10c.



(c)

Figure 4.10: The AFM measurement of pillar one with multi-layer graphene on top. (a) Depicts the error signal of the measurement. (b) Depicts the height measurement of pillar one. (c) The height profile along the blue arrow of the height plot.

4.3.3 Pillar two

Pillar two seen in SEM is shown in figure 4.11. This second pillar has again some sharp lines around it, these are interpreted as folds of graphene. The graphene does not touch the pillar or substrate everywhere. Irregularities are visible around the flake and are interpreted as carbon features as a residue of the graphene stamping process.

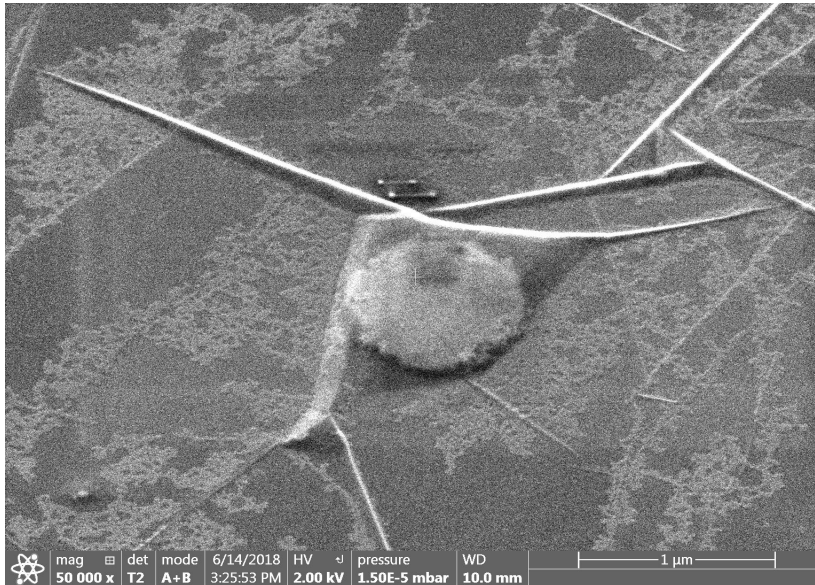
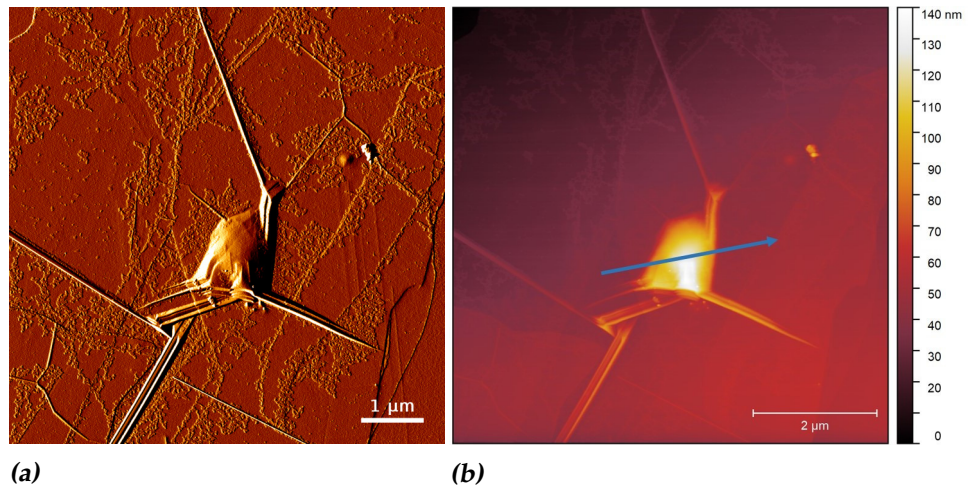


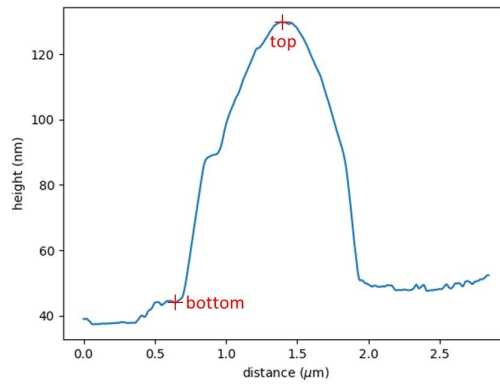
Figure 4.11: Pillar two with multi-layer graphene on top as seen in SEM, image taken under 45°. The folding of the graphene is visible on the flake.

This same pillar two is viewed with AFM. The AFM image is rotated about 180° w.r.t. the SEM image, figure 4.11. In the AFM image the folding of the graphene flake is again visible. The blue arrow corresponds to the location and direction of the height plot in figure 4.12c. Both AFM images show measurement artifacts. This is visible as double lines which do not appear in the SEM image.



(a)

(b)



(c)

Figure 4.12: AFM results of pillar two with multi-layer graphene on top. (a) The error signal of the measurement of pillar two. (b) Height measurement of pillar two. (c) Height profile along the blue arrow in the height measurement.

4.3.4 Pillar three

The third pillar is shown in figure 4.13, this figure is made using SEM. This image shows the pillar and the flake of graphene over it. Some sharp lines are visible and are interpreted as folding lines of graphene. The graphene does not touch the pillar or substrate everywhere. The contrast of the figure is enhanced to be able to see these folding lines and the pillar clearly.

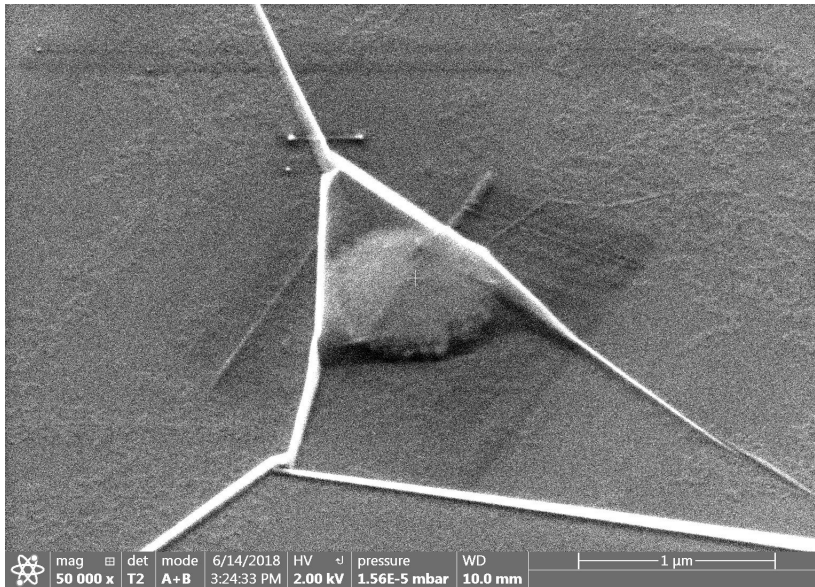


Figure 4.13: Pillar three with multi-layer graphene on top as seen in SEM, image taken under 45°. The contrast of the image is enhanced to be able to see the graphene and the pillar clearly.

The same pillar is viewed with AFM, and is shown in figure 4.14. In this AFM image the folding of the graphene is again visible. This figure is rotated about 180° w.r.t. figure 4.13. This image shows some double lines which do not appear in the SEM image. These are due to measurement artifacts of the AFM process. The blue arrow represents the location and direction of the height plot of this pillar. This height plot is shown in figure 4.14c.

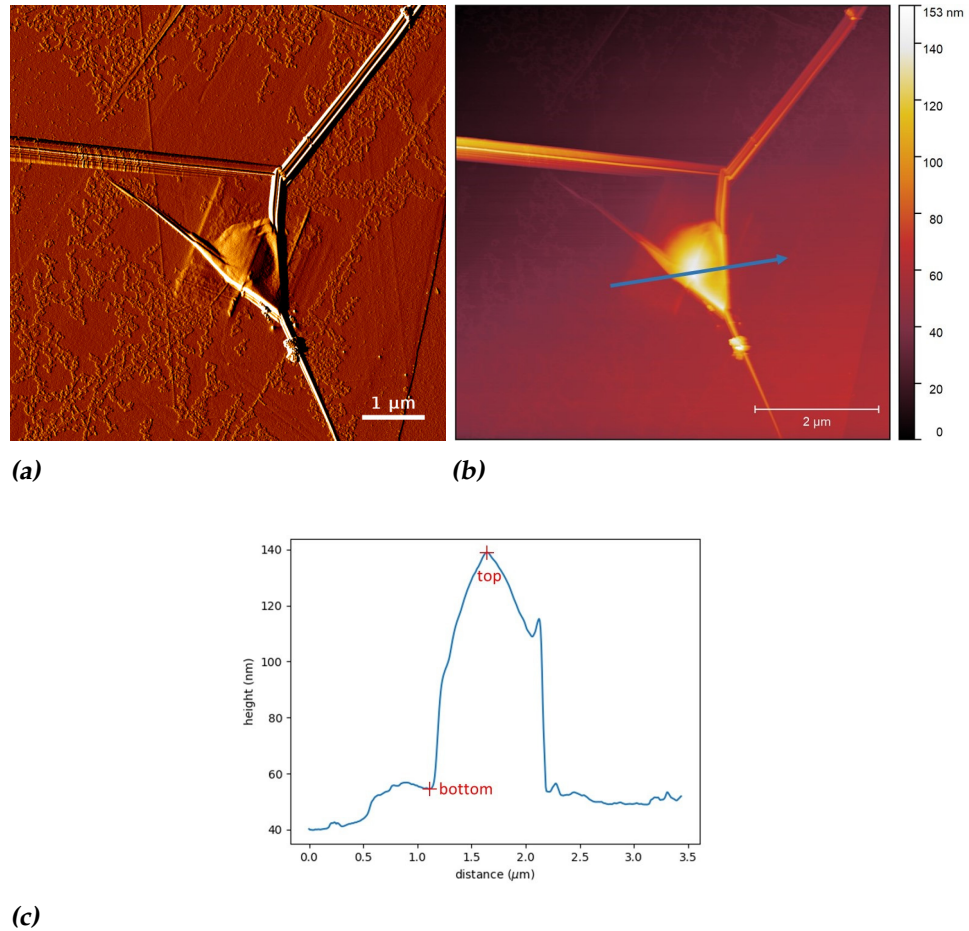


Figure 4.14: The AFM measurement of pillar three with multi-layer graphene on top. (a) The error signal of the AFM measurement. (b) Height measurement of pillar three. (c) The height plot along the blue arrow in the height measurement.

4.4 Expected angle

The expected angle is calculated using the corresponding height plots of the pillars. The top height and the bottom height of the pillars are used, together with the corresponding distance between them. This is done to characterize the height of the pillar and the average angle the flake makes w.r.t. horizontal. The height plots are shown in figure 4.10c, 4.12c and 4.14c. The height plots also include markers at the top and bottom positions of the pillars.

The coordinates of the top and bottom positions of the height plots are displayed in table 4.1. The coordinates are used to calculate the average angle and the height of the pillars.

The average angle (β) of the pillars is calculated using equation 4.1.

| Pillar no. | h_{top} (nm) | h_{bottom} (nm) | d_{top} (μm) | d_{bottom} (μm) |
|------------|----------------|-------------------|-----------------------|--------------------------|
| one | 116 | 43 | 1.31 | 0.63 |
| two | 129 | 44 | 1.38 | 0.65 |
| three | 139 | 54 | 1.63 | 1.12 |

Table 4.1: The coordinates of the top and bottom positions from the height plots in figure 4.10c, 4.12c and 4.14c. The coordinates are used to calculate an average angle and the height of the pillars.

$$\beta = \arctan\left(\frac{h_{top} - h_{bottom}}{d_{top} - d_{bottom}}\right) \quad (4.1)$$

The calculated average angles are displayed in table 4.2 together with the height difference between the bottom and the top of each flake.

| Pillar no. | height (nm) | β ($^{\circ}$) |
|------------|-------------|------------------------|
| one | 73 | 6.1 |
| two | 85 | 6.6 |
| three | 85 | 9.5 |

Table 4.2: The average angles the flake makes w.r.t. horizontal. The height of the flake is shown too. The calculation of the average angle is done via equation 4.1

From this last table the conclusion that all flakes have an average angle between 5° and 10° is drawn.

Results

5.1 LEEM results

To determine the local tilt angles the method of first gaussian smoothening and after that taking the brightest pixel is applied, as described in subsection 3.3.3. In our LEEM measurements, the same aperture is always used. This aperture has a size of 338 nm. The colored plotted areas are one third of this size. This is done to be able to see all measuring points clearly.

Of all four measured locations four plots are made. The first is an overview of the area, second is the magnitude of the angle plotted over the overview image, third is the direction of the angle plotted over the overview image and fourth is both magnitude and direction plotted as a vector over the overview. The vectors are always plotted in arbitrary units and the starting point of the vector is the point which has the calculated local tilt angle. In all four areas some irregular dark grey spots are visible. These are interpreted as carbon features and are a residue of the graphene stamping process.

The used landing energy to make the real space images is shown in each right upper corner of each image. These are: flat area 5.0 eV, pillar one 3.7 eV, pillar two 3.4 eV and pillar three 3.4 eV. The landing energy to take the diffraction images are different for each area. These were: flat area 19.4 eV, pillar one 13.2 eV, pillar two 16.2 eV and pillar three 16.4 eV. All real space images are made in bright field mode in the LEEM.

The used stepsize is 100 nm in both direction for the flat area, pillar one and pillar three. Pillar two was measured with a stepsize of 200 nm in both directions.

In the overview of pillar one, two and three there is both light grey visible and dark grey. The light grey is graphite and the dark grey area is the substrate; silicon.

5.1.1 Flat area

The absolute angle is shown in figure 5.1b with a color plot. The figure shows angles between zero and one degree. The angle increases to half a degree in the middle of the image. Figure 5.1c depicts the direction of the angle in the flat area. The part in the middle with the half a degree magnitude now has about the same direction, at -50° .

In figure 5.1d the combination of magnitude and direction of the angles is shown. No clear pattern is visible of the vectors. There are about five long arrows corresponding to the larger angles of figure 5.1b.

5.1.2 Pillar one

The magnitude of the measured angles are shown in figure 5.2a. The magnitudes are all smaller than ten degrees. The magnitudes show a circle of larger angles around the pillar. The middle of this circle has a smaller magnitude. Around this circle of larger magnitude the angles are mostly purple. So around the pillar the magnitude varies between zero and about two degrees.

The direction of the angle is plotted in figure 5.2c. This figure shows a circle in direction around the pillar. On the parts around the pillar the direction is mostly in the purple/pink regime.

In figure 5.2d the angles are shown as vectors. Around the pillar very small vectors are shown. At the pillar appear larger vectors.

5.1.3 Pillar two

The overview image with the magnitude of the angles is plotted in figure 5.3b. The magnitudes are all smaller than 12 degrees. The magnitude shows a circle of larger magnitude around pillar two. On the top of the pillar smaller angles are illustrated.

The direction of the angles are calculated for the region of pillar two, depicted in figure 5.3c. The direction does not show a clear circle around the pillar.

The information of the magnitude and the direction of the angles is combined in figure 5.3d. On and at the edge of the pillar the magnitudes are a lot larger than around these places.

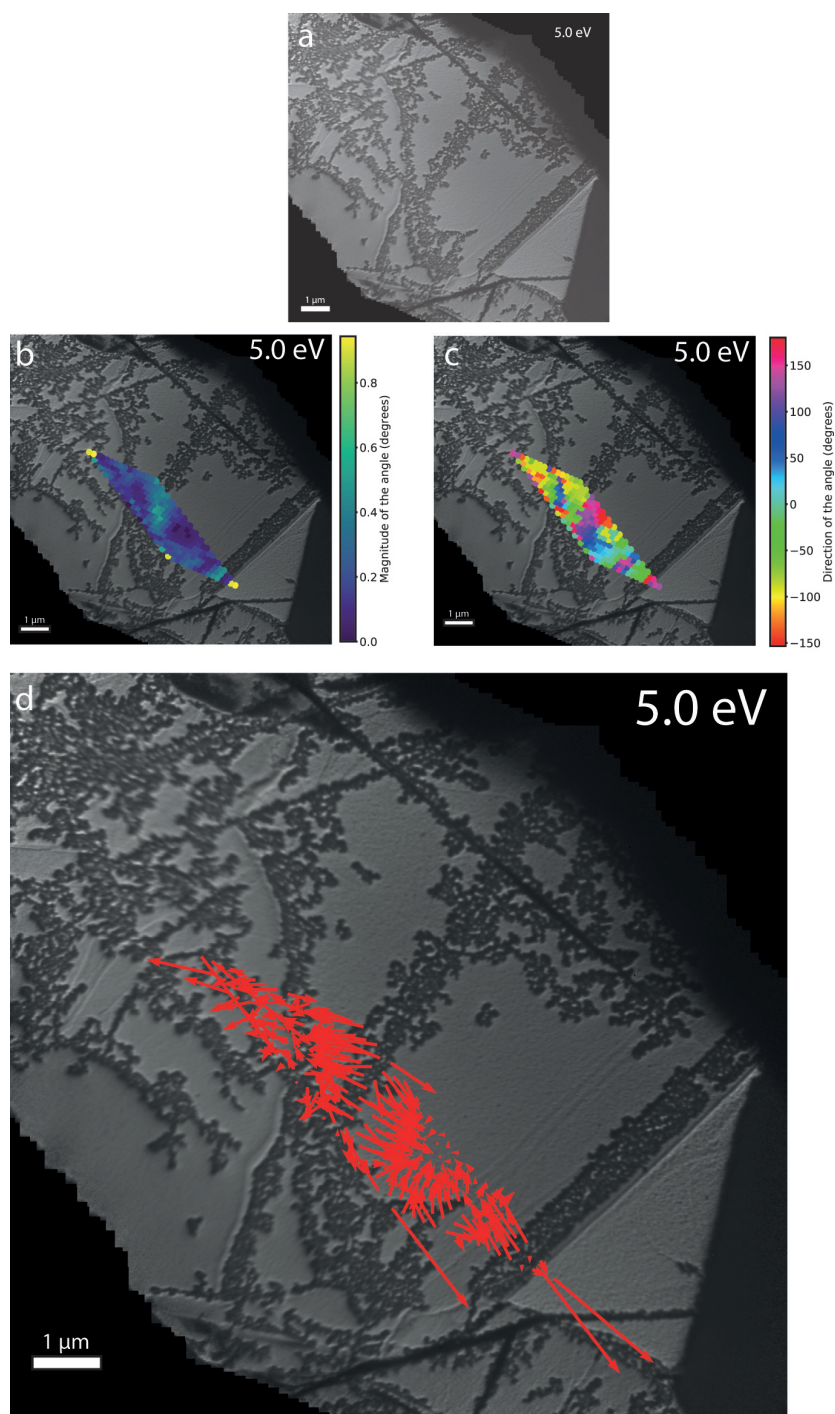


Figure 5.1: LEEM measurement of the flat area. The real space images are made in bright field mode using a landing energy of 5.0 eV, the diffraction images are made using a landing energy of 19.4 eV. The local tilt angles for the flat area are calculated. (a) Overview of the flat area, (b) The magnitude of the angle, (c) The direction of the angle and (d) Both magnitude and direction plotted as a vector on an arbitrary scale.

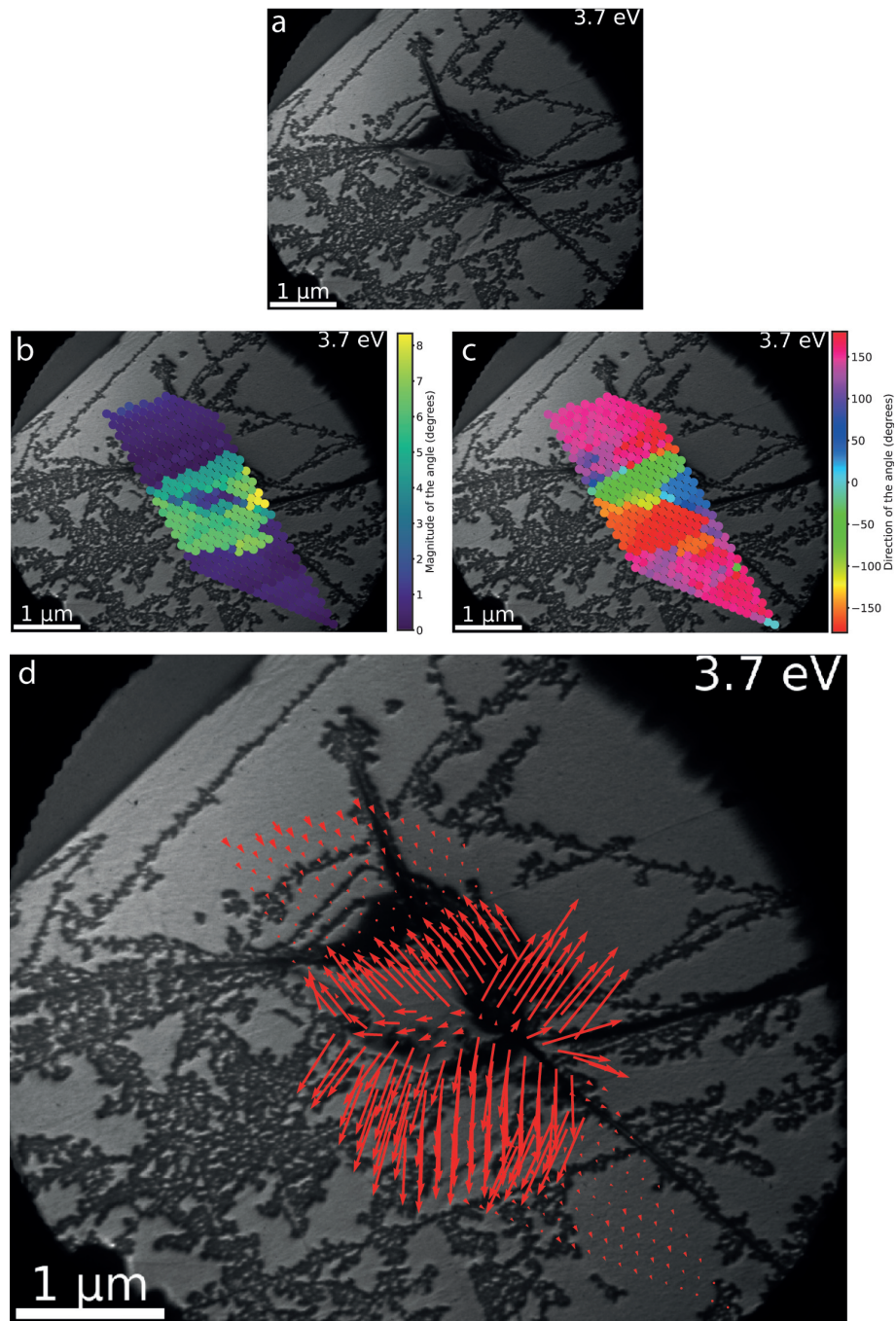


Figure 5.2: Images taken in LEEM in bright field mode using a landing energy of 3.7 eV for the real space images and 13.2 eV for the diffraction images. The local tilt angles are calculated for pillar one. (a) Overview of pillar one, (b) The magnitude of the angle, (c) The direction of the angle and (d) Both magnitude and direction plotted as a vector on an arbitrary scale.

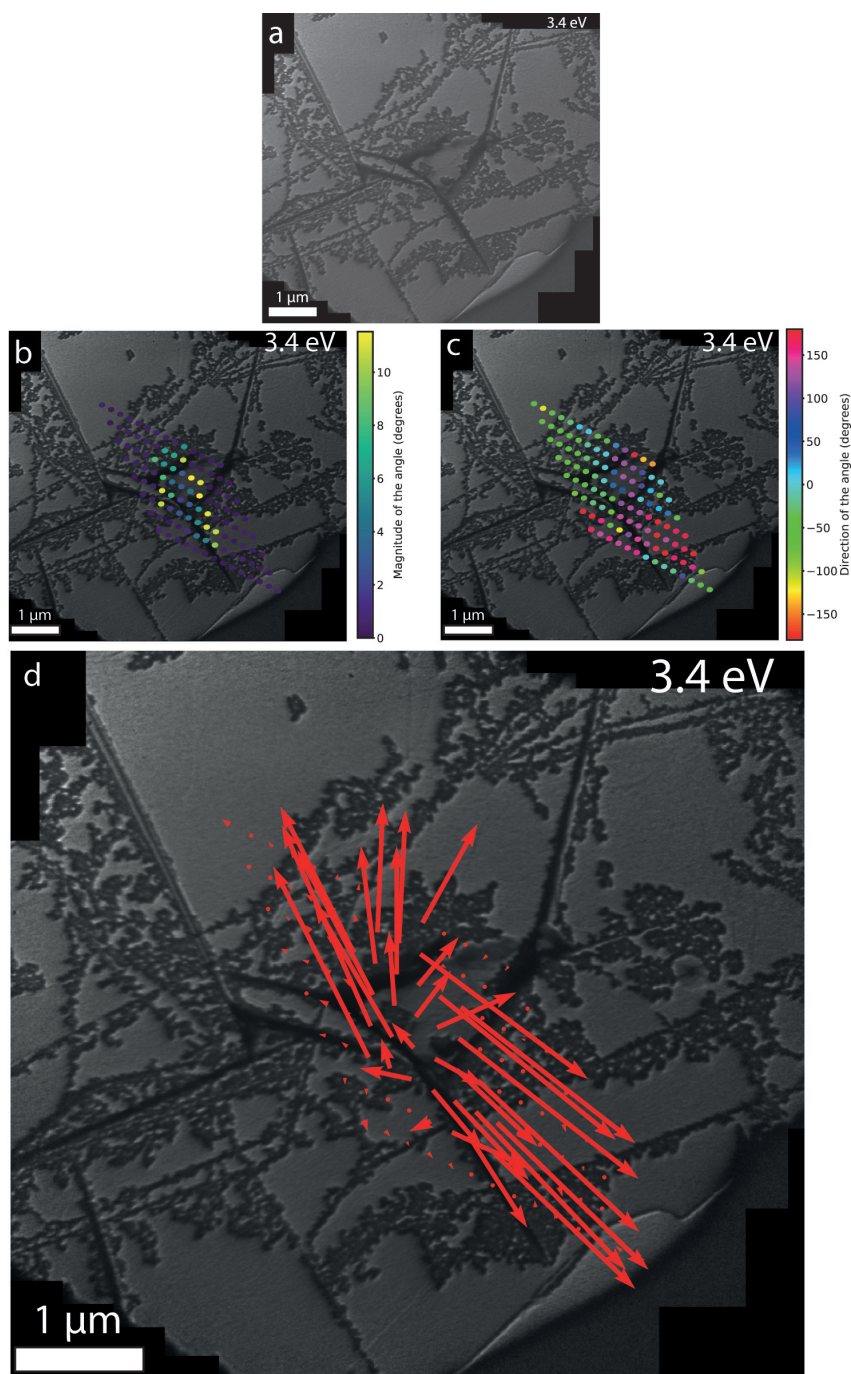


Figure 5.3: The real space images for pillar two were made using a landing energy of 3.4 eV in bright field mode and the diffraction images were made using a landing energy of 16.2 eV. The local tilt angles in the region of pillar two are determined. (a) Overview of pillar two, (b) The magnitude of the angle, (c) The direction of the angle and (d) Both magnitude and direction plotted as a vector on an arbitrary scale.

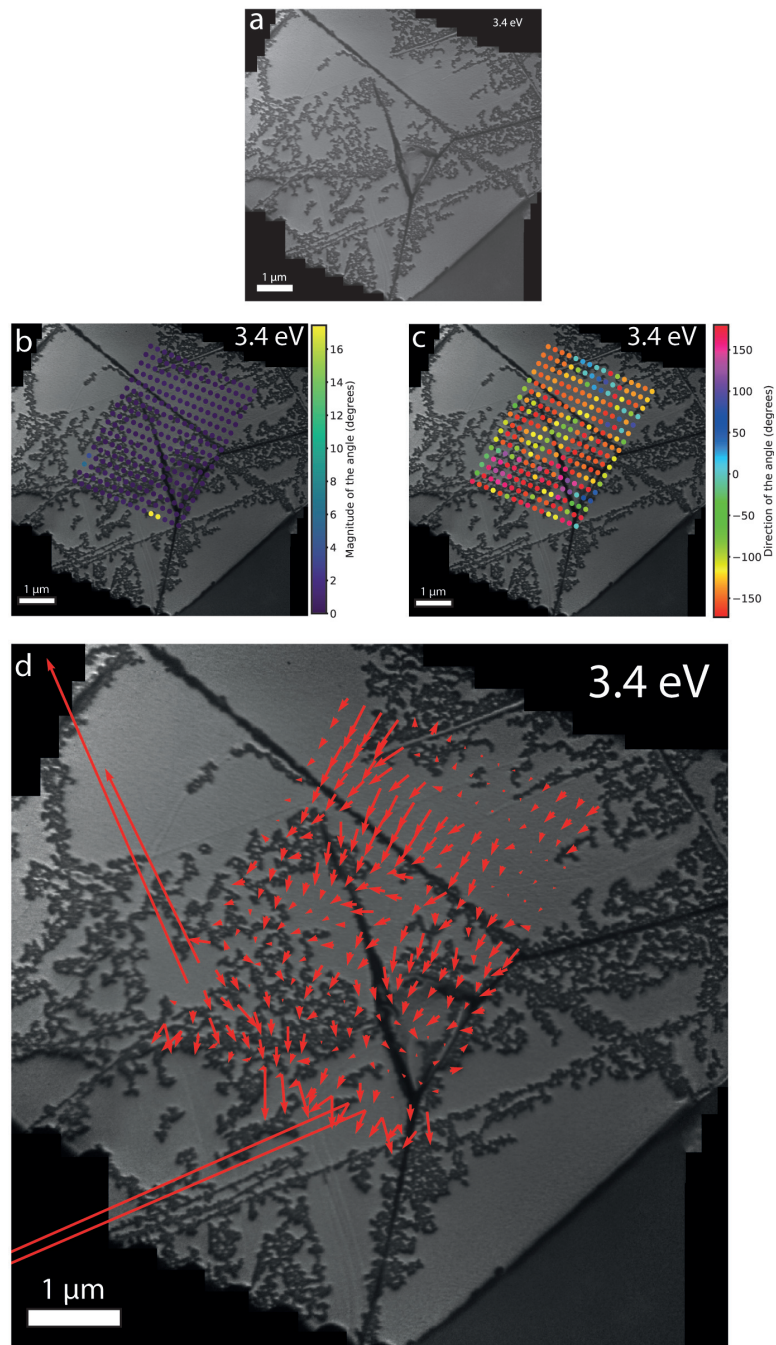


Figure 5.4: LEEM measurement of the local tilt angles in the region of pillar three. The real space images were made using a landing energy of 3.4 eV and the diffraction images were made with a landing energy of 16.4 eV. The values for the local tilt angles around pillar three are calculated. (a) Overview of pillar three, (b) The magnitude of the angle, (c) The direction of the angle and (d) Both magnitude and direction plotted as a vector on an arbitrary scale.

5.1.4 Pillar three

The magnitude of the angle is calculated and plotted in figure 5.4b. This figure shows only four points not being purple. All angles are smaller than 18° .

The calculated direction of the angles is shown in figure 5.4c. The directions make a full circle together.

The magnitude and direction are combined in figure 5.4d. This image shows a lot small vectors and four notable large vectors. The magnitude of the vectors are on an arbitrary scale.

The four points with large magnitude are numbered by their frame number in figure 5.5.

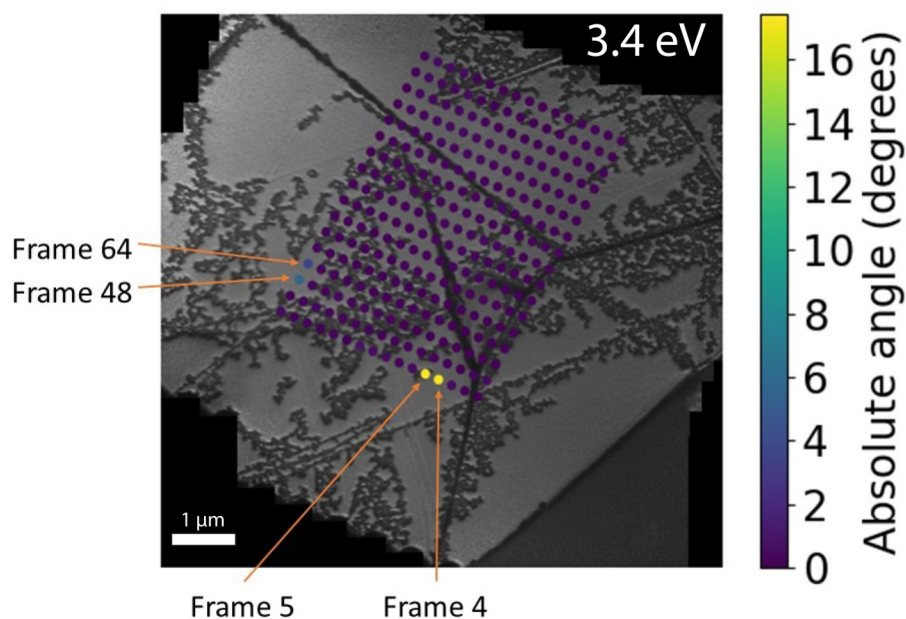


Figure 5.5: Four points with notable large local tilt angle magnitude in the measurement sequence of pillar three. The points are labeled by their frame number.

The corresponding four diffraction frames are listed in figure 5.6.

Figure 5.6 shows the detected brightest pixels of frame 4 and 5 which are pixels in the first order diffraction spot. So these two frames can be ignored, since the movement of the zeroth order diffraction spot needs to be determined. In frame 48 and 64 pixels inside the zeroth order diffraction spot are found to be the brightest. Therefore these frames cannot be ig-

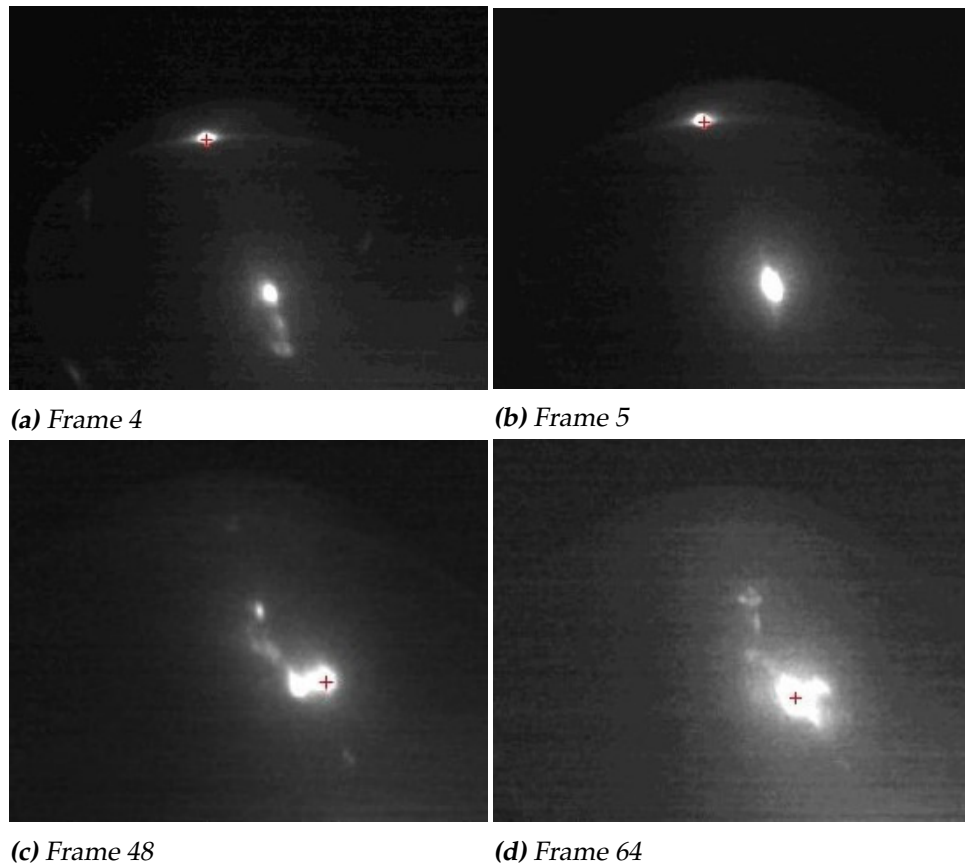
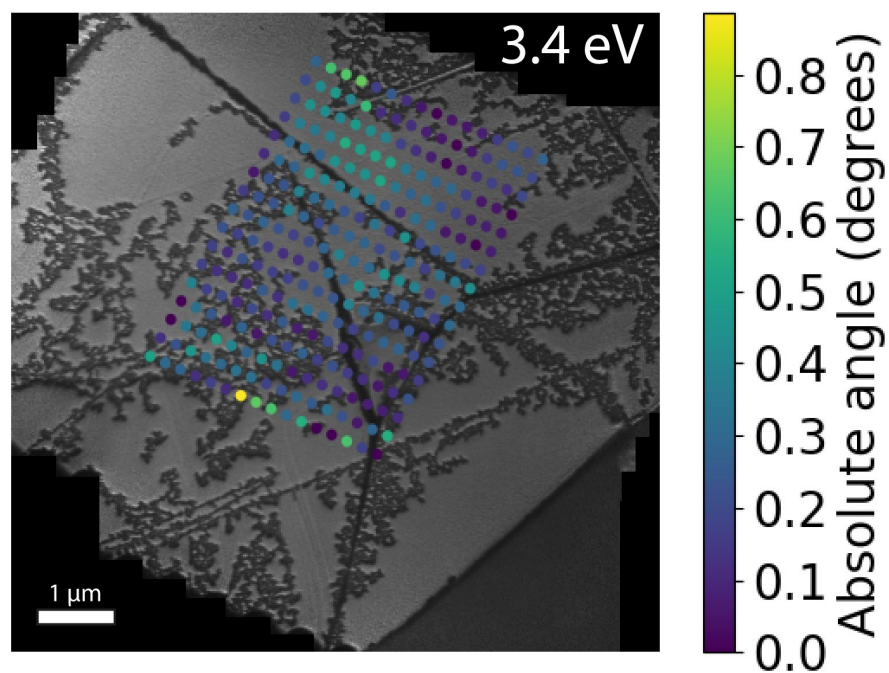
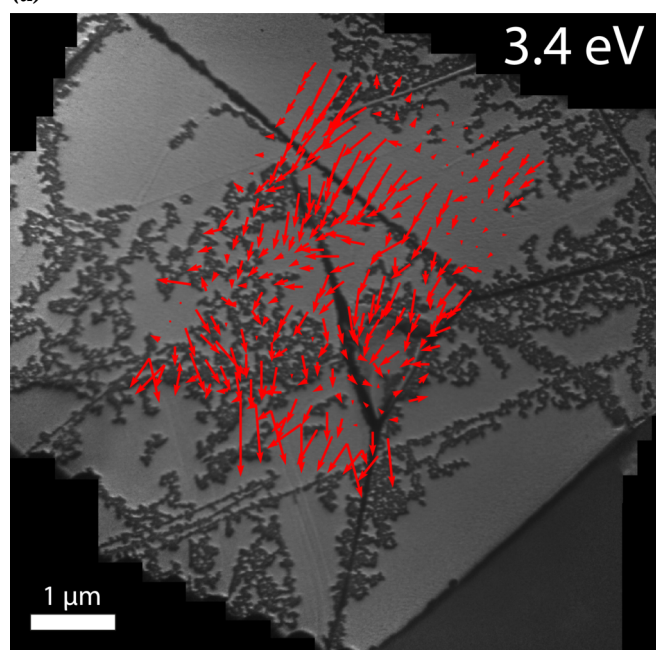


Figure 5.6: The four diffraction images as designated in figure 5.5. These are the four measured angles with calculated magnitude larger than 3° .

nored, but they stretch out the scalebar, so in order to make the magnitude of the other points visible they are filtered out. Since frame 4 and 5 can be ignored and frame 48 and 64 are such that they stretch the scalebar, these four angles are manually filtered out. The filter sets all angles larger than 3° to zero. The result is visible in figure 5.7. The direction of the angle is not affected by the filtering. The new vector plot is visible in figure 5.7b.



(a)



(b)

Figure 5.7: Filtered values for the angles for pillar three, all angles larger than 3° are set to zero. (a) Magnitude of the filtered angles and (b) filtered magnitude and direction plotted as a vector on an arbitrary scale.

Chapter 6

Discussion

In both the plots of the first and second pillar there seems to be a shift in the locations where the angles are plotted. The vector plot of pillar one seems to be shifted by 750 nm to the right bottom, and the vector plot of pillar two seems to be shifted by half a micro meter downwards. These shifts are probably caused by the aperture. A possible explanation for this shift is magnetic impurities in the aperture drive. This will cause the electron beam to bend, so effectively the angle measurement is done at a different location than expected by the real space images. This is probably also the case for the flat area and the third pillar, but there is no clear pattern visible in these two plots, so no shift can be detected in that data.

To find the diffraction spot a gaussian smoothening is applied to the diffraction images. Therefore half the size of the diffraction spot is a measure of the uncertainty of the method in both magnitude and direction determination. This changes for each diffraction image, but during the measurements this was about a degree.

6.1 Flat area

In the flat area angles up to a degree were measured. The AFM image does also contain no tilt in the measured region. There are five points with the magnitude of one degree. This is all within the uncertainty of one degree. The rest of the magnitudes show a rather random pattern. The expectation for a flat part is that the direction would not change. Therefore a random pattern is a logical outcome. At a flat surface an overall direction is not expected. So the outcome of the measurement matches with the expectation. The AFM data confirms that there is no overall preferred direction.

6.2 Pillar one

Both magnitude and direction show a circle around the first pillar. This circle is around 6° in magnitude. This corresponds to the average angle of 6.1° . On the top of the pillar the magnitude also decreases to two degree or less. The different tilted areas (so in between two folds of graphene) do also show a single magnitude. This is confirmed by the AFM data, the AFM image shows areas between two folds which are more or less a flat plane. The direction of the angle also shows areas with the same direction. This is again confirmed by these AFM planes with the same orientation. So the developed measurement method works for pillar one.

6.3 Pillar two

The angle magnitude of the second pillar looks like a circle around the pillar. This is confirmed by the AFM data. Some spots do have an angle up to 11° , but most are around 6° or 8° . The average angle was 6.6° , so angles up to 11° are off by about a factor 2.

The LEEM measurement shows roughly a circle around the pillar in the direction of the angle. This is a logic result when compared to the AFM data. A few areas with (about) the same direction are visible. These are the areas with the smaller magnitudes. But the direction does not show a clear transition along the sides of the pillar. This may be caused by the stepsize. The stepsize was 200 nm, in contrast to the three other stepsizes of 100 nm. The vector plot shows vectors from the top of the pillar pointing to the bottom of the pillar. So for pillar two the magnitude calculation worked out to be fine, but the orientation seems to be not fully correct.

6.4 Pillar three

The magnitude of the angle shows here four points which are larger than 3° . The rest of the points do have an angle of one degree or less. The pillar is not visible in the magnitude data.

The direction of the angle does not show a pattern. The colors seem to appear very random. The height measurement of the angle shows very steep edges at the sides of the pillar. Therefore an average angle of 9.5° was calculated. This average angle does clearly not show up in the magnitude plot nor the direction plot.

The calculated magnitude could be caused by the steep step of the flake at the edges of the pillar. Although the flake is not flat between these step edges as can be seen in the AFM height plot.

The changes in the measuring algorithm will probably not cause this, because the changes only involve the movement of the sample. Therefore

only the location of the measurement is different than it was before (i.e. more square like). This does not affect the diffraction pattern at all. In the diffraction images a clear specular spot is visible. So further investigation needs to be done in order to provide an answer to what is going on. The developed measurement method did not work for the third pillar.

Conclusion & outlook

The overall conclusion of this experiment is that the measurement method needs to be further developed in order to ensure it works. The method works as expected in two of the four cases. In one of the cases the method worked half, the magnitude worked fine but the direction not. In the last case the method did not work. Therefore the suggestion is to repeat the measurement of pillar two with a stepsize of 100 nm and completely repeat the measurement of pillar three.

The spatial resolution of this method is equal to the size of the aperture, so a circle of 338 nm in diameter. The angle resolution in both magnitude and direction depends on the method to find the diffraction spot. In this experiment half the size of the diffraction spot was taken to be the uncertainty of both the magnitude and the direction of the local tilt angle. This was calculated to be a degree.

The method can also be extended to super resolution. This can be done by comparing a diffraction frame with the one before. This gives information about the relative change in intensity of the visible diffraction spots. So two measurement locations in real space will provide three measured local angles; the angle of the overlapping part can be determined separately.

Acknowledgments

First of all I am very lucky I did my research in the group of Sense Jan van der Molen. All people in this group have always been very kind to me and helpful. The people always brought inspiration to me and ensured that I could get a quick reply if necessary. First of all I want to thank Sense Jan, he ensured the possibility to do this research in his group. Vera has helped me a lot on a daily basis and led me in the right direction. She took me through the whole process to make a success out of this process.

A special thanks to Tobias and Johannes for being helpful all the time, especially when I had a question and Vera was not around. This ensured I was not stuck with a problem for a long time. Furthermore it was a pleasure to have two other bachelor students in the group. This led to conversations about all three of our projects and we learned a lot from each other. I want to thank Lennard for helping me out with several coding issues and his insights to improve my code. A special thanks goes to Jean Paul for being my fellow office worker. We helped each other all the time during the project and we have laughed a lot during these five months. He created a nice working environment and I can not imagine having a better neighbor.

Allemaal hartelijk dank voor de fijne tijd in de groep!

Bibliography

- [1] *SURFACE STATES AND RECTIFICATION have a*, Physical Review **71**, 717 (1947).
- [2] R. Koppera, D. Voiry, S. E. Yalcin, W. Jen, M. Acerce, S. Torrel, B. Branch, S. Lei, W. Chen, S. Najmaei, J. Lou, P. M. Ajayan, G. Gupta, A. D. Mohite, and M. Chhowalla, *Metallic 1T phase source/drain electrodes for field effect transistors from chemical vapor deposited MoS₂*, APL Materials **2** (2014).
- [3] S. Song, D. H. Keum, S. Cho, D. Perello, Y. Kim, and Y. H. Lee, *Room Temperature Semiconductor-Metal Transition of MoTe₂ Thin Films Engineered by Strain*, Nano Letters **16**, 188 (2016).
- [4] K.-A. N. Duerloo, Y. Li, and E. J. Reed, *Structural phase transitions in two-dimensional Mo- and W-dichalcogenide monolayers*, Nature Communications **5** (2014).
- [5] A. Andringa, *A Novel Technique to Study Surface Profiles of Two-Dimensional Materials in LEEM*, PhD thesis, University of Leiden, 2017.
- [6] D. Metten, G. Froehlicher, and S. Berciaud, *Monitoring electrostatically-induced deflection, strain and doping in suspended graphene using Raman spectroscopy*, 2D Mater **4** (2017).
- [7] R. M. Tromp, J. B. Hannon, W. Wan, A. Berghaus, and O. Schaff, *A new aberration-corrected, energy-filtered LEEM/PEEM instrument I. Operation and results*, Ultramicroscopy **110**, 852 (2013).
- [8] R. M. Tromp, J. B. Hannon, W. Wan, A. Berghaus, and O. Schaff, *A new aberration-corrected, energy-filtered LEEM/PEEM instrument II. Operation and results*, Ultramicroscopy **127**, 25 (2013).
- [9] S. H. Simon, *The Oxford Solid State Basics*, chapter 13.1, pages 127 – 134, Oxford University Press, New York, fourth edition, 2013.

- [10] R. Cherian and P. Mahadevan, *Size dependence of lattice constants of semiconductor nanocrystals*, Appl. Phys. Lett. Applied Physics Letters **92** (2008).